International Journal of Thermophysics (2024) 45:169
https://doi.org/10.1007/s10765-024-03472-7

Thermal Conductivity Characterization of High Oleic Vegetable Oils Based Hybrid Nanofluids Formulated Using GnP, TiO_2, MoS_2, Al_2O_3 Nanoparticles for MQL Machining

Anthony Chukwujekwu Okafor[1] · Tobechukwu Kingsley Abor[1] · Saidanvar Esanjonovich Valiev[1] · Ignatius Echezona Ekengwu[1] · Abiodun Saka[2] · Monday U. Okoronkwo[2]

Received: 23 October 2024 / Accepted: 12 November 2024 / Published online: 23 November 2024

Abstract

This paper presents the results of thermal conductivity characterization of six high oleic soybean oil (HOSO) and four high oleic canola oil (HOCO)-based hybrid nanofluids formulated with four types of nanoparticles (Graphene nanoplatelet (xGnP), TiO_2, MoS_2, and Al_2O_3) at nanoparticles wt% concentration from 1 % to 7 % in 1 % increment using the two-step method for use in MQL machining of difficult-to-cut metals. Thermal conductivity of the formulated hybrid nanofluids were measured using Thermtest Transient Hot Wire Liquid Thermal Conductivity Meter at temperatures from 25 °C to 75 °C in increment of 10 °C. Obtained results showed that thermal conductivity of all nanofluids decreases linearly with temperature, while the thermal conductivity enhancement increases nonlinearly with increase in wt% concentration, following second order polynomial. At 7-wt% nanoparticle concentration, hybrid nanofluids xGnP-TiO_2/HOSO gave the highest thermal conductivity enhancement (109.73 % and 103.31 % at 25 and 75 °C) followed by xGnP-TiO_2/HOCO (101.36 % and 97.52 % at 25 °C and 75 °C), xGnP-MoS_2/HOCO (101.36 % and 97.52 % at 25 °C and 75 °C), xGnP-MoS_2/HOSO (96.3 % and 96.89 % at 25 °C and 75 °C), xGnP-Al_2O_3/HOCO (91.62 % and 83.23 % at 25 °C and 75 °C), xGnP-Al_2O_3/HOSO (91.25 % and 83.23 % at 25 °C and 75 °C). xGnP hybrid nanofluids are recommended for MQL machining. TiO_2–MoS_2/HOSO, TiO_2–MoS_2/HOCO, MoS_2–Al_2O_3/HOSO, TiO_2–Al_2O_3/HOSO hybrid nanofluids gave the lowest thermal conductivities and are not recommended as base fluids due to their insignificant thermal conductivity enhancement. Thermal conductivity of the hybrid nanofluids is lower than that of mono-nanofluids, but there are other inherent properties that could be beneficial.

Extended author information available on the last page of the article

Keywords Graphene nanoplatelet-Al_2O_3–MoS_2–TiO_2-nanoparticles · High oleic vegetable oils · Hybrid-nanofluid · Minimum quantity lubrication machining · Thermal conductivity characterization · Transient hot wire method

1 Introduction

High-strength materials like Inconel 718, titanium alloy Ti–6Al–4V and Compacted Graphite Iron (CGI) are used in aerospace and automotive industries due to their high specific strength, durability, and damage tolerance [1]. Machining these difficult-to-cut materials faces challenges due to high heat and friction generated at the cutting zone, leading to severe tool wear, poor surface finish and efficiency [2]. Cutting fluids are used to reduce temperature and friction at the cutting zones. Thermal conductivity and viscosity are the most important properties of the cutting fluids that determine their suitability and performance in machining. Higher thermal conductivity in cutting fluids results in a better heat removal during the machining process [3]. Lower viscosity provides better cooling performance but leads to a lack of lubrication between tool edge and work piece, which leads to poor surface finish and increased tool wear [4]. One of the vastly used cutting fluids is conventional emulsion coolant (CEC) that is environmentally unfriendly, causes irritation, skin deceases, and health issues upon frequent contact [5], but due to its high thermal conductivity [6] it is still used in machining. Moreover, aerosols are generated during machining while using CEC that cause severe corrosion of the metal [7]. Environmental regulations have pushed machining industries to consider environmentally friendly lubrication and cooling techniques [8]. In this regard, vegetable oils are being investigated for use as cutting fluids instead of CEC. Properties of vegetable oils are enhanced using nanoparticles dispersed in the base vegetable oil to form nanofluids for use in minimum quantity lubrication (MQL) machining [9]. MQL is a technique where a small amount of vegetable oil is sprayed to the machining zone. Cryogenic MQL has been developed [10–12] to overcome the heat problem, and cryogenic fluid in combination with MQL has been proposed but causes hardening of the materials that increase cutting forces and tool breakage due to sudden cooling. Nanofluid MQL proved to have better performance compared to conventional MQL in face milling of Inconel 718, where nanofluids MQL reduced surface roughness, temperature and power to 20.1 %, 14.7 % and 13.3 %, respectively [13]. Dispersion of graphene oxide nanoparticles in industrial metalwork coolant reduced the cutting temperature and friction force in machining of Ti–6Al–4V [14]. Thermal conductivity and viscosity of 43 nm aluminum oxide/water-based nanofluid was observed to increase with increase of volume concentration of nanoparticles at room temperature [15]. An increase of thermal conductivity by 7.4 % at 3 % of TiO_2-nanoparticle concentration with distilled water (DW) as base fluid (BF), where viscosity also increased more than predicted value using Einstein model have been observed [16]. Aluminum-, zinc- and copper-oxide/water ethylene glycol compound based nanofluids also did not show good agreement between experimental results and existing models [17]. Most of the cutting fluids reported in the literature are water, ethylene glycol and mineral oil based, but vegetable oil is receiving wide attention due to its

advantages over water, ethylene glycol and mineral oil. A review has shown that nanoparticles dispersion into mineral, vegetable and lubricating oil BF reduces surface roughness by 15 % to 25 %, cutting force by 32 % to 35 %, tool wear by 25 % to 30 % and coefficient of friction by 40–45 %, and increases tool life by 40 % to 65 % [18]. The influence of silicon carbide, copper, and diamond nanoparticles has been investigated using vegetable oils as BF in MQL end-milling of aluminum alloy [19]. MoS_2—soybean vegetable oil based nanofluids was used for MQL grinding of Grade 45 steel. 6 % concentration of MoS_2 in the BF showed the best tribological performance [20]. Improvement in cutting force and surface roughness compared to dry machining was reported. Soybean, palm, coconut, sunflower, and rice bran oils, impregnated with Al_2O_3, SiO_2, CuO, MoS_2, TiO_2, graphene, and carbon nanotube (CNT) nanoparticles show promising results [21–23]. Polystyrene (PS) was dispersed in DW that resulted in the reduction of thermal conductivity of the nanofluid by − 25 % due to PS' relatively low thermal conductivity compared to water-base fluid [24]. Therefore, to enhance thermal conductivity of nanofluid, it is important for the nanoparticle's thermal conductivity to be higher than that of the BF. Nanoparticles are classified as metallic or non-metallic, and the nanofluid formed could be conventional nanofluid (mono nanoparticle of the same average size) or hybrid nanofluid (multi-type nanoparticles of same or different average sizes). Hybrid nanofluids effect on engine oil has been studied by adding hybrid nanoparticles (MgO—Multi-Walled Carbon Nanotubes—MWCNT) [25]. Increasing hybrid nanoparticle mass concentration to 2 % at 50 °C, thermal conductivity increased by 65 %. Thermal conductivity and viscosity of MWCNT using a volume fraction of 0.05 % and deionized water as BF has been studied [26]. The result showed an enhancement of 36 % and 5.5 % in thermal conductivity and viscosity. The study on carbon quantum (C-dot), MXene and a hybrid MXene/C-dot nanofluids demonstrated that thermal conductivity of MXene nanofluid enhanced by 50 % over the BF reaching 1.003 $Wm^{-1}{\cdot}K^{-1}$ at 0.2-wt% concentration [27]. The hybrid MXene/C-dot demonstrated a lower enhancement of 42.2 % with thermal conductivity of 0.945 $Wm^{-1}{\cdot}K^{-1}$. Significant reduction 20.2 %, 21.3 %, 13.6 % of cutting forces in Fz, Fx, Fy and surface roughness of 33.4 % has been achieved for Al_2O_3-MWCNT hybrid nanofluid over Al_2O_3 mono nanofluid in turning of AISI 304 steel [28]. Minimum surface roughness ($Ra = 0.423$ µm) has been achieved at the lowest feed of 0.012 mm/z and highest cutting speed of 4150 rpm using Al_2O_3-MWCNT hybrid nanoparticle dispersed in BF comprising of 5 % Blasocut oil mixed with DW during milling of Ti–6Al–4V [29]. Dispersion of $AgNO_3$–graphene hybrid nanoparticles into water-based fluid improved thermal conductivity by 8.21, 15.37, and 23.59 % at 0.01, 0.02, and 0.03 wt% concentration of nanoparticles at 75 °C [30]. A critical review [31] have shown that hybrid nanofluids have better tribological features and machining performance in comparison with some mono nanofluids. Machining performance of Inconel X-750 superalloy was evaluated in milling [32], in which vegetable oil-based MQL three hybrid nanoparticles containing hexagonal boron nitride (hGN), graphite (Grpt) and MoS_2 (hBN/Grpt, hBN/MoS_2 and Grpt/MoS_2) were dispersed also, hBN/Grpt, hBN/MoS_2, and Grpt/MoS_2 had 22.97 %, 25.15 % and 30.10 % higher viscosity (at 40 °C), 16.01 %, 21.05 % and 22.12 % higher thermal conductivity, respectively. However, dispersed nanoparticles agglomerate during storage

over time. Surfactants are added to keep nanoparticles dispersed for a longer period. Three surfactants (Sodium Dodecyl Sulfate (SDS), Cetyltrimethylammonium Bromide (CTAB) and Oleic Acid) with different sonication time have been studied on $Mg(OH)_2$—water-based nanofluid, where all the samples with different sonication time have shown to be stable by the 7th day, while on the 30th day, only the samples with 30-min and 50-min sonication times for CTAB surfactant showed better stability followed by SDS and Oleic Acid [33]. Investigation has shown that Al_2O_3, MoS_2, and TiO_2—high oleic soybean oil based nanofluid remained stable for a week then started to agglomerate within 2 weeks [34]. From the literature reviewed so far, vegetable oil-based hybrid nanofluids showed better performance compared to DW, petroleum oil and ethylene glycol-based nanofluids. Therefore, current research investigates thermal conductivity of hybrid nanofluids formulated using four different types of nanoparticles—Titanium oxide (TiO_2), Molybdenum disulfide (MoS_2), Aluminum oxide(Al_2O_3), and Graphene Nanoplatelets (xGnP) with varying nanoparticle weight percentage (wt%) concentration (1 wt%, 2 wt%, 3 wt%, 4 wt%, 5 wt%, 6 wt%, and 7 wt%) and temperature range (25 °C, 35 °C, 45 °C, 65 °C, and 75 °C) dispersed in high oleic soybean oil (HOSO) and HOCO base fluids. Since high oleic acid content acts as a surfactant that enhances stability of the nanofluids and has good thermal conductivity compared to other vegetable oils provides added advantage in the stability of dispersed nanoparticles in the base fluid. Al_2O_3, TiO_2, and MoS_2 nanoparticles of 30-nm diameter nanoparticle size, and Graphene Nanoplatelets xGnP (XG Sciences-USA) of 15-nm thickness were added and uniformly suspended in HOSO and HOCO to form six HOSO-based hybrid nanofluids: xGnP-TiO_2//HOSO, xGnP-MoS_2/HOSO, xGnP-Al_2O_3/HOSO, TiO_2–MoS_2/HOSO, TiO_2–Al_2O_3/HOSO and MoS_2–Al_2O_3/HOCO and four HOCO-based hybrid nanofluids: xGnP-TiO_2/HOCO, xGnP-MoS_2/HOCO xGnP-Al_2O_3/HOCO, and TiO_2–MoS_2/HOCO to investigate the effect of nanoparticle type of the same size, nanoparticle wt% concentration, and temperature on thermal conductivity before recommending them for use in MQL machining of difficult-to-cut metals. Thermal conductivities of the formulated hybrid nanofluids are measured and characterized vs temperature and wt% concentration.

2 Theoretical Background of Thermal Conductivity Measurement

Thermal conductivity is measured using Thermtest transient hot wire (THW-L2) Liquid Thermal Conductivity Meter based on ASTM standard D7896-19 in the range 0.01 to 2 $Wm^{-1}{\cdot}K^{-1}$, where small volume of liquid is tested for thermal conductivity accurately in less than 2 s in a single measurement. The THW sensor consists of a thin heating Alumel wire of 0.126 mm in diameter and 60 mm in length and is completely inserted into the sample and A platinum RTD for independently measuring the temperature of the sample. The THW-L2 sensor wire is heated by constant current source q then the temperature rise (°C) vs time (sec) is automatically recorded by tracking the change in electrical resistance of the wire as shown in Fig. 1a. Total of 100 temperature rise points are measured with incremental time step of 0.011 s for a total time length of

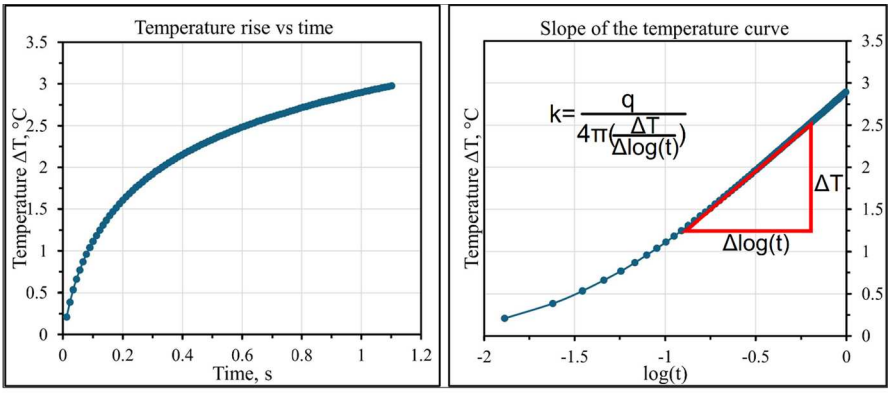

(a)-Temperature rise vs time (b)-Temperature rise vs Log(t)

Fig. 1 Determination of slope for thermal conductivity calculation

1.089 s. The slope a from the plot of temperature rise vs logarithm of time is used to calculate thermal conductivity k as shown in Eq. 1.

$$k = \frac{q}{4\pi a} \tag{1}$$

where, q—quantity of heating power supplied (mW), a—slope of the temperature rise (°C) vs logarithm of time (log(t)). The sample plot of the temperature rise vs logarithm of time that is used to find the slope is shown in Fig. 1b. The temperature rise vs logarithm of time stamp is taken for every temperature difference after the test. Then a linear trendline is fitted to find the tangent to the curve. Usually, the first few pairs of temperature rise vs log (t) (say 1 to 20 or 30 points) which fall on the nonlinear curve part are not used in plotting the temperature rise vs logarithm of time (log (t)). Since the heating wire must first heat itself before it heats the test sample, there is a nonlinearity between the temperature change and log(t) at the beginning of measurement. Then the nonlinearity disappears after a short while followed by a linear trend, but if the time is too long nonlinearity appears again. The nonlinearity at longer times is due to the appearance of convection. Therefore, measurement is taken only for 1 s. The thermal conductivity formula is only valid when nonlinearity is not present.

The lower the slope the higher the thermal conductivity of the material and vice versa.

The thermal conductivity enhancement percentage of the base fluid is calculated using Eq. 2.

$$\Delta k/_k = \frac{k_{\mathrm{nf}} - k_{\mathrm{bf}}}{k_{\mathrm{bf}}} \times 100 \tag{2}$$

where, Δk—thermal conductivity enhancement, k_{nf}—thermal conductivity of nanofluid, k_{bf}—thermal conductivity of the base fluid. For hybrid nanofluid, replace k_{nf} with k_{hnf} the thermal conductivity of hybrid nanofluid.

3 Materials and Methods

This section presents a brief description of the materials for the vegetable oil base fluids and nanoparticles investigated, formulation of mono and hybrid nanofluid, and thermal conductivity characterization with reference to temperature and nanoparticle wt% concentration and type. Based on the authors recent comparative study of seven vegetable oils: HOSO, HOCO, Low Oleic Soybean Oil (LOSO), Acculube LB2000, Olive Oil, Palm Oil, Coconut Oil and CEC, where HOSO and HOCO showed better performance as base fluid for MQL machining compared to other vegetable oils, HOSO and HOCO were used as based fluids to formulate hybrid nanofluids. Four different types of nanoparticles: TiO_2, MoS_2, Al_2O_3, and xGnP with varying nanoparticle wt% concentration (1 wt%, 2 wt%, 3 wt%, 4 wt%, 5 wt%, 6 wt%, and 7 wt%) were dispersed in HOSO and HOCO base fluids using two-step method to form six HOSO-based hybrid nanofluids: xGnP-TiO_2//HOSO, xGnP-MoS_2/HOSO, xGnP-Al_2O_3/HOSO, TiO_2–MoS_2/HOSO, TiO_2–Al_2O_3/HOSO and MoS_2–Al_2O_3/HOSO and four HOCO based hybrid nanofluids: xGnP-TiO_2/HOCO, xGnP-MoS_2/HOCO xGnP-Al_2O_3/HOCO, and TiO_2–MoS_2/HOCO.

3.1 Materials

HOSO was obtained from Archer Daniels Midland Inc (Decatur, IL, USA), while HOCO was obtained from Cargill Inc (Minneapolis, MN, USA). Vegetable oils are characterized by their fatty acid (FA) composition. Distinguishing features of oils from various sources are directly correlated with their length of the FA chains, ranging from 8 to 24 carbon atoms. A saturated fatty acid (SFA) has only one single bond in carbon chain. FA with a double bond is referred to as monounsaturated fatty acid. FA with several double bonds between carbon atoms, is referred to as polyunsaturated FAs. The FA composition of HOSO and HOCO used in formulating the hybrid nanofluids in this research are shown in Table 1. From Table 1, it is seen that HOSO has 74.5 % of Mono-Unsaturated Fatty Acid (MUFA) (Oleic Acid, C18:1), 13 % of SFA (Palmitic + Stearic Acids, C16:0 + C18:0) and 11 % of Poly-Unsaturated Acid (PUFA) (C18:2 and C18:3); while HOCO has 60 % of MUFA (Oleic Acid, C18:1), 4.02 % of SFA (Palmitic + Stearic Acids, C16:0 + C18:0) and 28.58 % of PUFA. HOSO and HOCO have high flash points of 325 °C and 340 °C, respectively, and iodine level of 80–90 and 111, respectively. The higher oleic acid content of 74.5 for HOSO compared to that of HOCO at 60 % indicates that HOSO would have a higher thermal conductivity compared to HOCO.

Based on extensive literature review, four different types of nanoparticles—titanium oxide (TiO_2), molybdenum disulfide (MoS_2), aluminum oxide (Al_2O_3) obtained from Nanoshell-UK and Graphene Nanoplatelets (xGnP-H5) from XG

Table 1 Fatty acid composition and physical properties of vegetable oils (HOSO and HOCO)

Vegetable oil base fluids	Fatty acid percentage composition					Physical properties			
	Saturated		Mono-unsaturated	Poly-unsaturated		Color	Flash point (* C)	Iodine value	Water soluble
	Palmitic C1 6:0	Stearic C18:0	Oleic C 18: 1	Linoleic C18:2	α-Linolenic C 1 S:3				
HOSO*	13		74.5	11		Light yellow	325	80–90	Insoluble
HOCO**	3.0	1.02	60	19.38	9.2	Light yellow	340	111	Insoluble

*Values for HOSO are provided by Archer Daniels Midland Company, Oil division, in their Product Data Sheet 780 700 Refined, Bleached, Deodorized, high oleic soybean oil

**Values for HOCO are provided by Cargill in their technical Product Data Sheet Agri-Pure 60 high oleic canola oil

Sciences-USA were selected for the formulation of hybrid nanofluids. Technical properties, specifications and cost of these nanoparticles investigated are shown in Table 2.

3.2 Preparation of Nanofluids and Hybrid Nanofluids

The preparation of nanofluids/hybrid nanofluids involves dispersing mono-nanoparticles/two different combinations of nanoparticles, at a given wt% concentration, into a base fluid to achieve a stable colloidal system. Fifty-mL empty plastic container, 20 mL of HOSO or HOCO base fluids and the calculated nanoparticle mass, M_{np} for a given nanoparticle wt% concentration, n, varying from 1 %, 2 %, 3 %, 4 %, 5 %, 6 %, and 7 %. The nanoparticle calculated weight values (in grams) for a given wt% concentration was weighed using Torbal AGN120 Analytical Balance scale with a resolution of 0.0001 g with a capacity of 120 g, repeatability of 0.0001 g, linearity of ± 0.0002 g with 1 % error in full scale reading. The empty container used for measuring the nanoparticle was weighed and the tare button was pressed to store the weight value. The mass of the nanoparticle (M_{np}) for a desired wt% conc. (n) of the nanofluid or hybrid nanofluid was computed using the 20-mL base fluid weight value. The measured wt% values of nanoparticles were dispersed into the 20-mL HOSO (HOCO) base fluid and thereafter inserted inside an ultrasonic bath and dispersed using Sonicor 1.5 gal. Digital ultrasonic cleaner, model: DS-150 TH, to sonicate the nanofluid/hybrid nanofluid for 90 min before measuring the thermal conductivity to disrupt the attraction between similar matters and further enhance the solid–liquid mixture. Each sample was sonicated before each thermal conductivity measurement.

The formula for calculating nanoparticle mass, M_{np}, for a given nanoparticle weight percent concentration is given as Eq. 3:

$$M_{np} = \left(\frac{n}{100 - n}\right) \times M_o \tag{3}$$

where, M_{np} = mass of nanoparticles in (g), n = wt% conc. of nanoparticle ranging from 1-wt%conc. to 7-wt%conc., M_o = Mass of 20 mL Oil in (g).

The descriptions of the six formulated hybrid nanofluids are given in Table 3 for HOSO and HOCO. From the four nanoparticles, xGnP, TiO_2, MoS_2 and Al_2O_3, for a given nanoparticle wt% concentration, two different combinations of nanoparticles were added to the base fluid in the amount n/2 wt% each. For example, for n = 1wt%, n/2 = 0.5 wt% of each combining nanoparticle was added, and so on.

4 Experimental Plan and Procedure for Characterization of Thermal Conductivity

Experimental plan for thermal conductivity measurement of HOSO and HOCO Base fluids and hybrid nanofluids vs nanoparticle weight percent concentration varying from 1 % to 7 % and temperature range from 25 °C to 75 °C is shown in Table 4 for

Table 2 Technical properties, specification and cost of nanoparticles investigated

Properties	MoS_{2*}	TiO_{2*}	Al_2O_{3*}	Graphene nanoplatelet (UK) (GnP)*	Graphene nanoplatelet USA (xGnP)-H5**
Purity	99.9	99.9+	99.9	99.5	
APS (dia.) (nm)	30	30	30		5 (microns)
Color	Black Powder	White	White	Black	Black Granules
Density ($g{\cdot}cm^{-3}$)	5.06	3.9	3.95–4.1	~2.3	2.2
Bulk density, ($g{\cdot}cm^{-3}$)	–	0.15–0.25	–	~0.10	0.03–0.1
Meting point (°C)	1185	1843	2072	3652–3679	
Electrical conductivity (Sm^{-1})	0.03–0.06	0.01–0.05	10^{-12} to 10^{-14}	80,000	10^7
Thermal conductivity ($Wm^{-1}{\cdot}K^{-1}$)	40–50	6.8–8.5	12–38	3000	3000, 6
Thermal expansion (mK^{-1})	10.5 (10^{-6}/K)	9–11 (10^{-6}/K)	5–10 (10^{-6}/K)	-8×10^{-6}/K	$4–6\times10^{-6}$
SSA ($m^2\ g^{-1}$)	45	> 30	15–20	20–40	50–80
pH	6–7	6–7	6.6	6–7	
Solubility in water	No	No	No	No	
Thickness (nm)	0.6 to 0.7	~30	~30	2–4	15
Lateral size (nm)	~30	~30	~30	~5 µm (+ − 3 %)	~5 µm
Layer flake	Multilayer	N/A	N/A	4–6 layers	
Tensile strength (MPa)	22 GPa			5 (GPa)	5 (MPa)
Tensile modulus (MPa)	270 GPa	230–285 (10^{-3})	330–400 (10^{-3})	~1 Tpa	1000
Price/unit ($/100 Gms.)	$800	$300	$500	$3000	$149

*Values for nanoparticle TiO_2, MoS_2, Al_2O_3, and GnP properties shown in the table were obtained from the technical datasheet supplied by Nanoshell-UK

**Values for nanoparticle xGnP properties shown in the table were obtained from technical datasheet supplied by XG Sciences Inc

Table 3 Description of hybrid nanofluids

Dispersed nanoparticles	Nanoparticle wt% concentration, *n*	Description of hybrid nanofluids
HOSO base fluid		
XGnP + TiO_2	n/2 + n/2 (n = 1, 2, 3, 4, 5, 6, 7)	XGnP-TiO_2/HOSO
XGnP + MoS_2	n/2 + n/2 (n = 1, 2, 3, 4, 5, 6, 7)	XGnP-MoS_2/HOSO
XGnP + Al_2O_3	n/2 + n/2 (n = 1, 2, 3, 4, 5, 6, 7)	XGnP-Al_2O_3/HOSO
TiO_2 + MoS_2	n/2 + n/2 (n = 1, 2, 3, 4, 5, 6, 7)	TiO_2–MoS_2/HOSO
TiO_2 + Al_2O_3	n/2 + n/2 (n = 1, 2, 3, 4, 5, 6, 7)	TiO_2–Al_2O_3/HOSO
MoS_2 + Al_2O_3	n/2 + n/2 (n = 1, 2, 3, 4, 5, 6, 7)	MoS_2–Al_2O_3/HOSO
HOCO base fluid		
XGnP + TiO_2	n/2 + n/2 (n = 1, 2, 3, 4, 5, 6, 7)	XGnP-TiO_2/HOCO
XGnP + MoS_2	n/2 + n/2 (n = 1, 2, 3, 4, 5, 6, 7)	XGnP-MoS_2/HOCO
XGnP + Al_2O_3	n/2 + n/2 (n = 1, 2, 3, 4, 5, 6, 7)	XGnP-Al_2O_3/HOCO
TiO_2 + MoS_2	n/2 + n/2 (n = 1, 2, 3, 4, 5, 6, 7)	TiO_2–MoS_2/HOCO

xGnP-TiO_2/HOSO hybrid nanofluids. Each hybrid nanofluid thermal conductivity characterization consists of eight experiments corresponding to eight nanoparticle wt% concentrations (0 %, 1 %, 2 %, 3 %, 4 %, 5 %, 6 %, and 7 %), corresponding individual nanoparticle wt% concentration, computed individual nanoparticle wt% value (g), total nanoparticle wt% value (g), nanofluid name, and measured thermal conductivity at various temperatures (25, 35, 45, 55, 65, and 75 °C) and wt% concentrations. Similar tables were made for all six HOSO-based hybrid nanofluids, and all four HOCO-based hybrid nanofluids.

Fifty-ml empty plastic container was weighed on Torbal AGZN120 Digital Analytic Balance, giving 7.4875 g 20 mL of HOSO Base Fluid (BF) was weighed giving a weight 16.228 g. Similarly, 20-mL HOCO Base Fluid was weighed giving a weight of 15.7586 g. For a 1 wt% xGnp-TiO_2 Nanofluid, 0.5 wt% of xGNP weighing 0.07956 g was mixed with 0.5 wt% of TiO_2 weighing 0.07956 g and HOCO 20 mL of HOCO base fluid weighing 15.7586 g. This mixture was sonicated for 90 min, after which it was taken to Thermtest THW TL-2 Thermal Conductivity Meter for measuring the thermal conductivity of the hybrid nanofluids. The same procedure was repeated for the other hybrid nanofluids prepared at various wt% concentration. The above preparations are applicable to all base fluids.

4.1 Thermal Conductivity Characterization

Thermal conductivity measurement of the base fluid and hybrid nanofluids were performed using Thermtest THW-L2 liquid Thermal Conductivity Meter based on ASTM standard D7896-19. The THW-L2 can measure thermal conductivity of fluids from 0.01 $Wm^{-1}{\cdot}K^{-1}$ to 2 $Wm^{-1}{\cdot}K^{-1}$ at temperature range of − 50 °C to 100 °C with accuracy and repeatability better than 5 % and 2 %, respectively. The actual repeatability of the thermal conductivity measurements for HOSO- and HOCO-based hybrid nanofluids varied from 0 % to 0.21 % with average of 0.07 %. Thermal conductivity of DW was measured and used to calibrate the

Table 4 Experimental plan for thermal conductivity measurement of hybrid nanofluids vs nanoparticle wt% concentration (1 % to 7 %) and temperature range (25 °C to 75 °C) for xGnP-TiO_2/HOSO

Exp. No.	Wt% Conc. xGnP-TiO_2	Nanofluid	Nanoparticle weight (g)	Total nanoparticle weight (g)	Nanofluid	Thermal conductivity ($Wm^{-1}\cdot K^{-1}$)					
						@25 °C	@35 °C	@45 °C	@55 °C	@65 °C	@75 °C
1.	0	HOSO-base fluid	0	0	HOSO-base fluid	0.17100	0.16800	0.16633	0.16500	0.16267	0.16033
2.	1	0.5 % TiO_2	0.0819	0.1639	TiO_2-xGnP/HOSO	0.19033	0.18433	0.17733	0.17300	0.16967	0.16600
		0.5 % xGnP	0.0819								
3.	2	1 % TiO_2	0.1615	0.3312	TiO_2-xGnP/HOSO	0.21100	0.20900	0.20367	0.19400	0.18833	0.18367
		1 % xGnP	0.1615								
4.	3	1.5 % TiO_2	0.25096	0.5019	TiO_2-xGnP/HOSO	0.21367	0.21133	0.20800	0.20433	0.20100	0.19700
		1.5 % xGnP	0.25096								
5.	4	2 % TiO_2	0.3381	0.6762	TiO_2-xGnP/HOSO	0.23567	0.23133	0.22600	0.22433	0.22033	0.21533
		2 % xGnP	0.3381								
6.	5	2.5 % TiO_2	0.4271	0.8541	TiO_2-xGnP/HOSO	0.26333	0.25967	0.25600	0.25267	0.21933	0.24767
		2.5 % xGnP	0.4271								
7.	6	3 % TiO_2	0.51793	1.03587	TiO_2-xGnP/HOSO	0.31767	0.31167	0.31100	0.30800	0.30500	0.30133
		3 % xGnP	0.51793								
8.	7	3.5 % TiO_2	0.61075	1.2215	TiO_2-xGnP/HOSO	0.35933	0.35633	0.35267	0.34500	0.33367	0.32733
		3.5% xGnP	0.61075								

THW-L2. Experimental setup of investigation of the effect of temperature ranging from 25 °C to 75 °C and nanoparticle wt% concentration on thermal conductivity is shown in Fig. 2. The setup consists of (1) Thermtest THW-L2 meter, (2) Echotherm Chilling/Heating Dry Bath, (3) sample container, (4) sample Cell, (5) THW Sensor which consists of a thin heating Alumel wire of 0.126 mm in diameter and 60 mm in length for heating the sample, and a platinum RTD for independently measuring the temperature of the sample, and (6) Desktop computer for programming automated experimental run and automatically record thermal conductivity for later retrieval and analysis. THW sensor is completely inserted into the sample cell, which is placed inside the sample container in Echotherm Chilling/Heating Dry Bath to be tested. Echotherm Chilling/Heating Dry Bath has an indicator that shows the actual temperature when it is reached and stabilized value. It is heated by constant current source (q) set at 80 mW then the temperature rise (°C) vs time (sec) is automatically recorded by tracking the change in electrical resistance of the wire. The slope of the plot of temperature rise vs logarithm of time is utilized to calculate thermal conductivity (k) as shown in Eq. 1.

For each experiment, 20 mL of nanofluid fluid was poured into the cylindrical groove connected to the sensor and allowed to sit for 15 min to stabilize. The heater was set to a measurement temperature of 20 °C and allowed to stabilize for 15 min before starting each measurement. Aluminum foil is used to minimize evaporation and prevent cooling of the samples during the thermal conductivity measurement. The experiments were conducted three times once the THW-L2 temperature sensor stabilized at 21.3 °C. A delay of 10 min was set between tests. The experiment was then initiated, and results were retrieved after 7 h. The experiments were repeated three times at each set temperature and the average was used for result analysis.

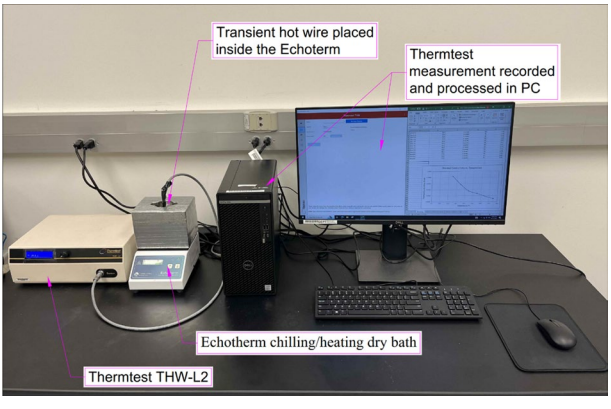

Fig. 2 Experimental setup for thermal conductivity measurement of hybrid nanofluids

5 Results and Discussions

Thermal conductivity of the base fluids and different hybrid nanofluids were determined at temperature range from 25 °C to 75 °C, at incremental interval of 10° and for varying wt% concentrations of 1 %, 2 %, 3 %, 4 %, 5 %, 6 %, and 7 %.

5.1 Thermal Conductivity of HOSO and HOCO Base Fluids

The measured thermal conductivity of HOSO and HOCO base fluids used for the formulation of mono nanofluids and hybrid nanofluids investigated in this study are shown in Fig. 3. It is observed that thermal conductivity of HOSO and HOCO are similar, both decrease linearly with increase in temperature. Thermal conductivities for HOSO are 0.1713 $Wm^{-1}{\cdot}K^{-1}$, 0.169 $Wm^{-1}{\cdot}K^{-1}$, 0.167 $Wm^{-1}{\cdot}K^{-1}$, 0.165 $Wm^{-1}{\cdot}K^{-1}$, 0.1633 $Wm^{-1}{\cdot}K^{-1}$, and 0.161 $Wm^{-1}{\cdot}K^{-1}$, at 25 °C, 35 °C, 45 °C, 55 °C, 65 °C, 75 °C, respectively, while that for HOCO are 0.171 $Wm^{-1}{\cdot}K^{-1}$, 0.169 $Wm^{-1}{\cdot}K^{-1}$, 0.167 $Wm^{-1}{\cdot}K^{-1}$, 0.165 $Wm^{-1}{\cdot}K^{-1}$, 0.163 $Wm^{-1}{\cdot}K^{-1}$, and 0.161$Wm^{-1}{\cdot}K^{-1}$ at 25 °C, 35 °C, 45 °C, 55 °C, 65 °C, 75 °C. Thermal conductivity for HOSO at room temperature, 25 °C and at 65 °C are slightly higher than that for HOCO. From the above results, it is indicated that either HOSO or HOCO could be used as they would produce similar performance.

5.2 xGnP-TiO_2/HOSO Hybrid Nanofluid

The thermal conductivities of xGnP-TiO_2/HOSO hybrid nanofluids measurements vs temperature, nanoparticle wt% concentration and % enhancement is shown in Fig. 4a and b, respectively. The Percentage enhancement of thermal conductivity vs wt% concentration is shown in Fig. 4c. It is observed from Fig. 4a that thermal conductivity decreases linearly with an increase in temperature for all wt%

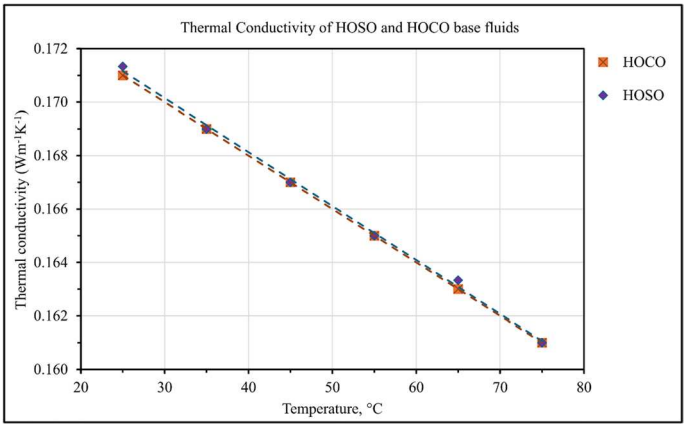

Fig. 3 Thermal conductivity vs temperature of HOSO and HOCO Base Fluids

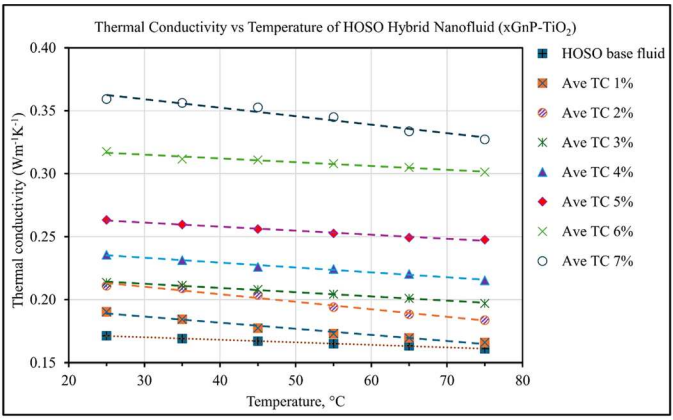

a. Thermal conductivity vs temperature.

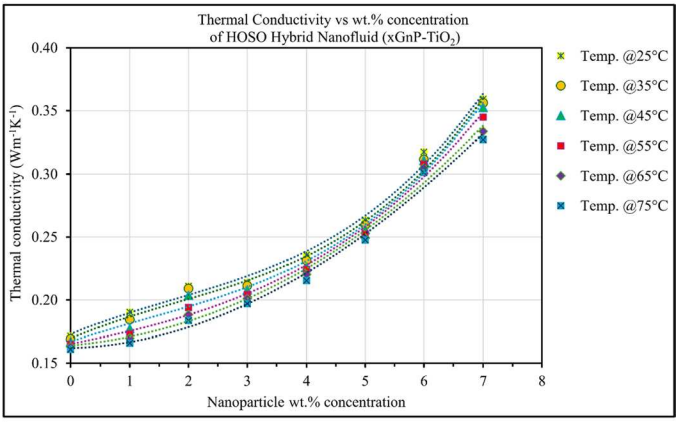

b. Thermal conductivity vs weight percentage concentration.

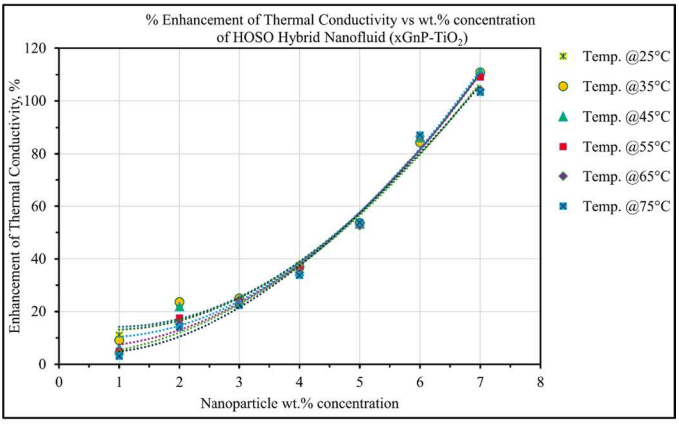

c. Enhancement of thermal conductivity vs wt.%.

Fig. 4 Thermal conductivity of xGnP-TiO_2/HOSO hybrid nanofluid and base fluid

concentration. Figure 4b shows that the addition of xGnP-TiO_2 hybrid nanoparticle to HOSO base fluid, thermal conductivity increases nonlinearly with increase in wt% concentration, following second order polynomial trend. At 1-wt% nanoparticle concentration, the thermal conductivity enhancement for xGnP-TiO_2/HOSO hybrid nanofluid were 11.09 %, 9.07 %, 6.19 %, 4.85 %, 3.88 %, and 3.11 % at 25 °C, 35 °C, 45 °C, 55 °C, 65 °C, and 75 °C, respectively as observed in Fig. 4c. At 7-wt% nanoparticle concentration, the thermal conductivity enhancement for xGnP-TiO_2/HOSO hybrid nanofluid were 109.73, 110.85, 111.18, 109.09, 104.29 and 103.31 at 25 °C, 35 °C, 45 °C, 55 °C, 65 °C, and 75 °C, respectively. The thermal conductivity of xGnP-TiO_2/HOSO hybrid nanofluid at 25 °C for 1-wt% and 7-wt% concentrations were 0.1903 $Wm^{-1}\cdot K^{-1}$ and 0.3593 $Wm^{-1}\cdot K^{-1}$, respectively. This increase in thermal conductivity is as the result of high thermal conductivity of xGnP-H5 nanoplatelet (3000 $Wm^{-1}\cdot K^{-1}$), the multilayered 2D plate-like structure, low density of 0.03 $g\cdot cm^{-3}$, the plate-like structure causes poor Van der Waals forces between the layers which makes the nanoparticles to be well dispersed and stable, the small thickness of 15 nm, and large surface area ($SSA = 50–80\ m^2\cdot g^{-1}$), in combination of TiO_2 small spherical particle size of 30 nm, low thermal conductivity of $6.8Wm^{-1}\cdot K^{-1}$ to $8.5Wm^{-1}\cdot K^{-1}$, moderate $SSA > 30\ m^2\cdot g^{-1}$, and average density of 3.9 $g\cdot cm^{-3}$.

5.3 xGnP-MoS_2/HOSO Hybrid Nanofluid

The thermal conductivity of xGnP-MoS_2/HOSO hybrid nanofluids measurements vs temperature and nanoparticle wt% concentration is shown in Fig. 5a and b, respectively. The Percentage enhancement of thermal conductivity vs wt% concentration is shown in Fig. 5c. It is observed from Fig. 5a that thermal conductivity decreases linearly with an increase in temperature for all wt% concentration. Figure 5b shows that the addition of xGnP-MoS_2 hybrid nanoparticle to the base fluid, thermal conductivity increases nonlinearly with increase in wt% concentration, following second order polynomial trend. At 1-wt% nanoparticle concentration, the thermal conductivity enhancement for xGnP-MoS_2/HOSO hybrid nanofluid were 14.98 %, 14.4 %, 10.77 %, 8.89 %, 7.76 %, and 7.45 % at 25 °C, 35 °C, 45 °C, 55 °C, 65 °C, and 75 °C, respectively as observed in Fig. 5c. At 7-wt% nanoparticle concentration, the thermal conductivity enhancement for xGnP-MoS_2/HOSO hybrid nanofluid were 96.3 %, 94.67 %, 92.81 %, 94.75 %, 95.31 %, and 96.89 % at 25 °C, 35 °C, 45 °C, 55 °C, 65 °C, and 75 °C, respectively. It is also observed that at higher wt% concentration from 5-wt% to 7-wt% concentration there is rapid enhancement, and the impact of temperature is minimized. The thermal conductivity of xGnP-MoS_2/HOSO hybrid nanofluid at 25 °C for 1-wt% and 7-wt% concentrations were 0.197 $Wm^{-1}\cdot K^{-1}$ and 0.34 $Wm^{-1}\cdot K^{-1}$, respectively. This increase in thermal conductivity is the result of high thermal conductivity of xGnP-H5 nanoplatelet (3000 $Wm^{-1}\cdot K^{-1}$), the multilayered structure, low density of 0.03 $g\cdot cm^{-3}$ which makes the nanoparticle to be well dispersed and stable, small thickness of 15 nm, and large surface area ($SSA = 50–80\ m^2\cdot g^{-1}$), and in combination of MoS_2 small particle

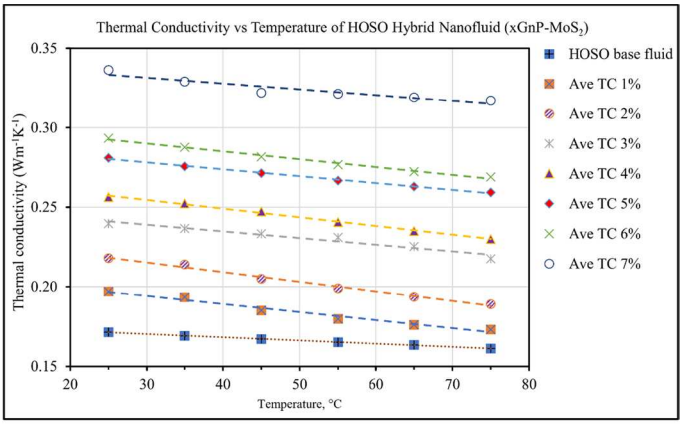

a. Thermal conductivity vs temperature.

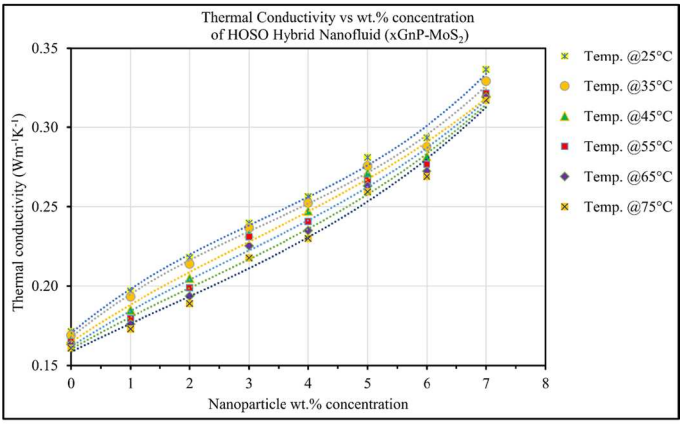

b: Thermal conductivity vs weight percentage concentration.

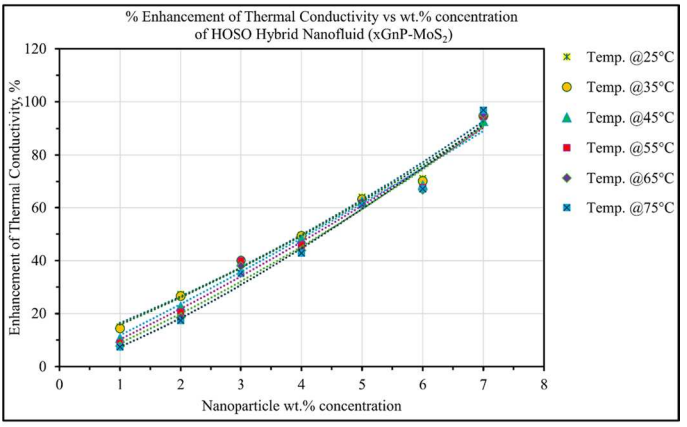

c. Enhancement of thermal conductivity vs wt.% concentration.

Fig. 5 Thermal conductivity of xGnP-MoS_2/HOSO hybrid nanofluid and base fluid

size of 30 nm, thermal conductivity of 40 $Wm^{-1}\cdot K^{-1}$ to $50Wm^{-1}\cdot K^{-1}$, moderate SSA = 45 $m^2\cdot g^{-1}$, and average density of 5.06 $g\cdot cm^{-3}$.

5.4 xGnP-Al_2O_3/HOSO Hybrid Nanofluid

The thermal conductivity of xGnP-Al_2O_3/HOSO hybrid nanofluids measurements vs temperature and nanoparticle wt% concentration is shown in Fig. 6a and b, respectively. The Percentage enhancement of thermal conductivity vs wt% concentration is shown in Fig. 6c. It is observed from Fig. 6a that thermal conductivity decreases linearly with an increase in temperature for all wt% concentration. Figure 6b shows that the addition of xGnP-Al_2O_3 hybrid nanoparticle to the base fluid, thermal conductivity increases nonlinearly with increase in wt% concentration, following second order polynomial trend. At 1-wt% nanoparticle concentration, the thermal conductivity enhancement for xGnP-Al_2O_3/HOSO hybrid nanofluid were 14.98 %, 14.0 %, 11.37 %, 9.29 %, 7.75 %, and 7.4 % at 25 °C, 35 °C, 45 °C, 55 °C, 65 °C, and 75 °C respectively as observed in Fig. 6c. At 7-wt% nanoparticle concentration, the thermal conductivity enhancement for xGnP-Al_2O_3/HOSO hybrid nanofluid were 91.25 %, 89.94 %, 88.02 %, 86.26 %, 84.08 %, and 83.23 % at 25 °C, 35 °C, 45 °C, 55 °C, 65 °C, and 75 °C, respectively. It is also observed that at 3 wt%, 4 wt%, and 6 wt% concentration the impact of temperature is minimized. The thermal conductivity of xGnP-Al_2O_3/HOSO at 25 °C for 1-wt% and 7-wt% concentrations were 0.197 $Wm^{-1}\cdot K^{-1}$ and 0.33 $Wm^{-1}\cdot K^{-1}$, respectively; and at 25 °C for 1-wt% and 7-wt% concentrations were 0.173 $Wm^{-1}\cdot K^{-1}$ and 0.30 $Wm^{-1}\cdot K^{-1}$, respectively. This increase in thermal conductivity is a result of high thermal conductivity of xGnP-H5 nanoplatelet ($3000Wm^{-1}\cdot K^{-1}$), the multilayered structure, low density of 0.03 g/cm^3 which makes the nanoparticle to be well dispersed and stable, small thickness of 15 nm, and large surface area (SSA = 50–80 m^2/g), and in combination of Al_2O_3 small particle size of 30 nm, moderate thermal conductivity of $12Wm^{-1}\cdot K^{-1}$ to $38Wm^{-1}\cdot K^{-1}$, low SSA = 15–20 $m^2\cdot g^{-1}$, and average density of 3.95 $g\cdot cm^{-3}$ to 4.1 $g\cdot cm^{-3}$.

5.5 TiO_2–MoS_2/HOSO Hybrid Nanofluid

The thermal conductivity of TiO_2–MoS_2/HOSO hybrid nanofluids measurements vs temperature and nanoparticle wt% concentration is shown in Fig. 7a and b, respectively. The percentage enhancement of thermal conductivity vs wt% concentration is shown in Fig. 7c. It is observed from Fig. 7a that thermal conductivities are very low compared to nanofluids containing xGnP and decrease linearly with an increase in temperature for all wt% concentration. Figure 7b shows that the addition of TiO_2–MoS_2 hybrid nanoparticle to the base fluid, thermal conductivity increases very slowly and nonlinearly with increase in wt. % concentration, following second order polynomial trend. At 1-wt% nanoparticle concentration, the thermal conductivity enhancement for TiO_2–MoS_2/HOSO hybrid nanofluid were 0.78 %, 0.97 %, 0.998 %, 0.81 %, 0.61 %, and 0.62 % at 25 °C, 35 °C, 45 °C, 55 °C, 65 °C, and 75 °C, respectively as observed in Fig. 7c. At 7-wt% nanoparticle concentration, the

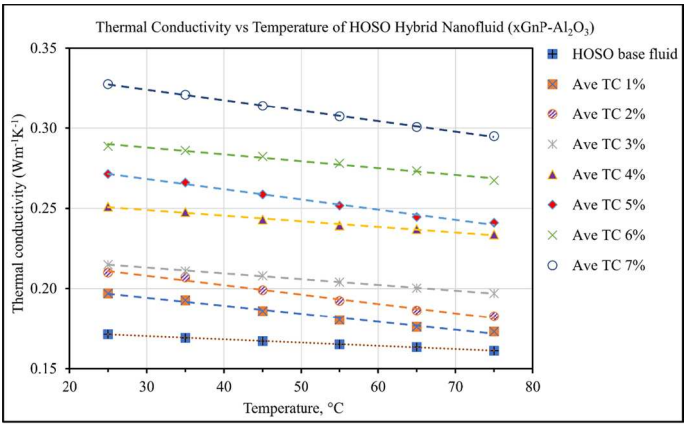

a. Thermal conductivity vs temperature.

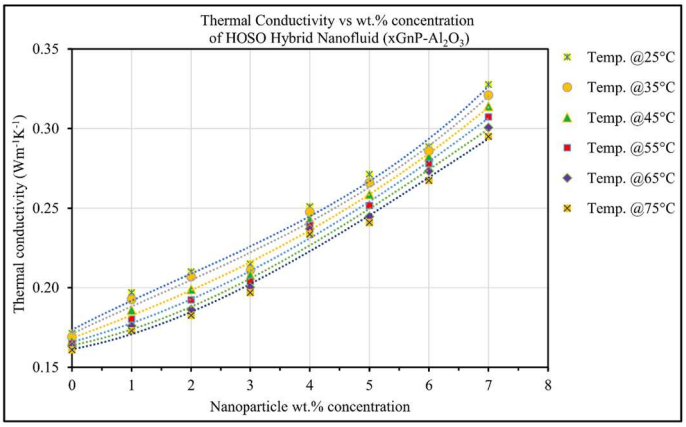

b. Thermal conductivity vs weight percentage concentration.

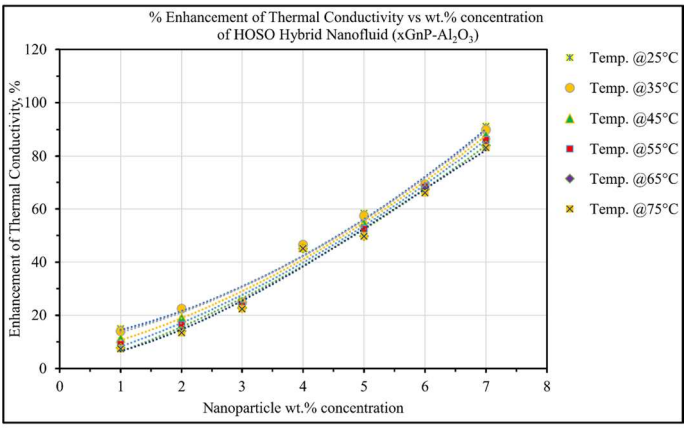

c. Enhancement of thermal conductivity vs wt.% concentration.

Fig. 6 Thermal conductivity of xGnP-Al_2O_3/HOSO hybrid nanofluid and base fluid

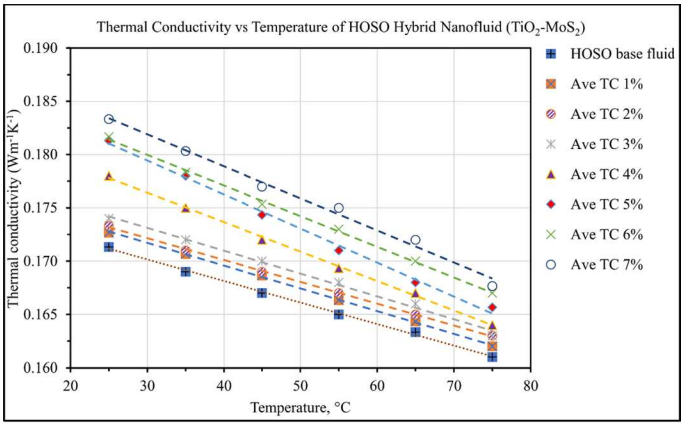

a. Thermal conductivity vs temperature.

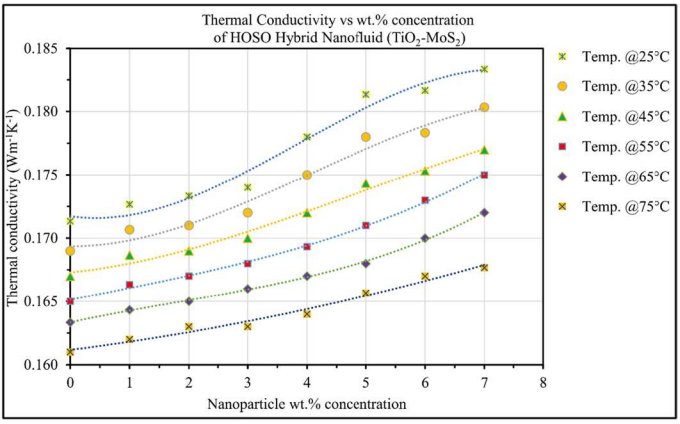

b. Thermal conductivity vs weight percentage concentration.

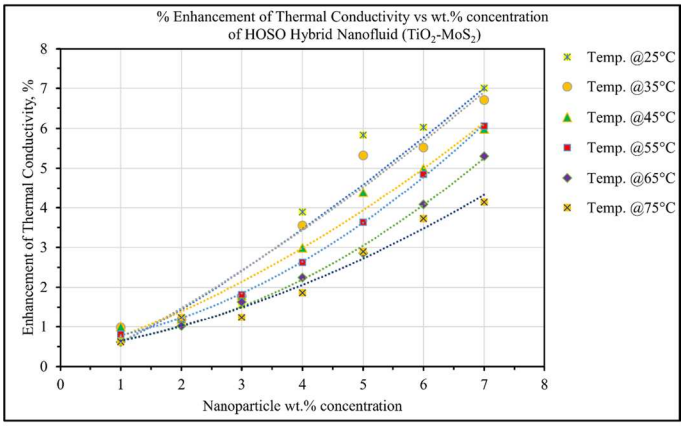

c. Enhancement of thermal conductivity vs wt.% concentration.

Fig. 7 Thermal conductivity of TiO_2–MoS_2/HOSO hybrid nanofluid and base fluid

thermal conductivity enhancement for TiO_2–MoS_2/HOSO hybrid nanofluid were 7.0 %, 6.71 %, 6.99 %, 6.06 %, 5.31 %, and 4.14% at 25 °C, 35 °C, 45 °C, 55 °C, 65 °C, and 75 °C, respectively. It is also observed that at 1 wt%, 2 wt%, and 3 wt% concentration the effect of temperature is insignificant, but at 4 wt%, 5 wt%, 6 wt%, and 7 wt% concentration the temperature effect is very significant. The thermal conductivity of TiO_2–MoS_2/HOSO at 25 °C for 1-wt% and 7-wt% concentrations were 0.173 $Wm^{-1}{\cdot}K^{-1}$ and 0.183 $Wm^{-1}{\cdot}K^{-1}$, respectively; and at 75 °C for 1-wt% and 7-wt% concentrations were 0.162 $Wm^{-1}{\cdot}K^{-1}$ and 0.168 $Wm^{-1}{\cdot}K^{-1}$ respectively. This low thermal conductivity and low enhancement implies there is no synergistic relationship between the two metallic and non-metallic oxides. Both nanoparticles TiO_2 and MoS_2 have small particle size of 30 nm, moderate thermal conductivity of 6.8 $Wm^{-1}{\cdot}K^{-1}$ to 8.5 $Wm^{-1}{\cdot}K^{-1}$ and 40 $Wm^{-1}{\cdot}K^{-1}$ to 50$Wm^{-1}{\cdot}K^{-1}$ respectively, and low SSA > 30 $m^2{\cdot}g^{-1}$ and 45 $m^2{\cdot}g^{-1}$, respectively and average density of 3.9 $g{\cdot}cm^{-3}$ and 5.06 $g{\cdot}cm^{-3}$, respectively.

5.6 TiO_2–Al_2O_3/HOSO Hybrid Nanofluid

The thermal conductivity of TiO_2–Al_2O_3/HOSO hybrid nanofluids measurements vs temperature and nanoparticle wt% concentration is shown in Fig. 8a and b, respectively. The percentage enhancement of thermal conductivity vs wt% concentration is shown in Fig. 8c. It is observed from Fig. 8a that thermal conductivities are very low compared to hybrid nanofluids containing xGnP and decrease linearly with increase in temperature for all wt% concentration. Figure 8b shows that the addition of TiO_2–Al_2O_3 hybrid nanoparticle to the base fluid, thermal conductivity increases very slowly and nonlinearly with increase in wt% concentration, following second order polynomial. At 1-wt% nanoparticle concentration, the thermal conductivity enhancement for TiO_2–Al_2O_3/HOSO hybrid nanofluid were 0.194 %, 0.099 %, 0.3 %, 0.18 %, 0.11 %, and 0.08 % at 25 °C, 35 °C, 45 °C, 55 °C, 65 °C, and 75 °C respectively as observed in Fig. 8c. At 7-wt% nanoparticle concentration, the thermal conductivity enhancement for TiO_2–Al_2O_3 hybrid nanofluid were 6.81 %, 6.31 %, 5.39 %, 4.65 %, 3.67 %, and 3.42 % at 25 °C, 35 °C, 45 °C, 55 °C, 65 °C, and 75 °C respectively This low thermal conductivity and low enhancement implies there is no synergistic relationship between the two metallic and non-metallic oxides. Both nanoparticles TiO_2 and Al_2O_3 have small particle size of 30 nm, moderate thermal conductivity of 6.8 $Wm^{-1}{\cdot}K^{-1}$ to 8.5 $Wm^{-1}{\cdot}K^{-1}$ and 12 $Wm^{-1}{\cdot}K^{-1}$ to 38 $Wm^{-1}{\cdot}K^{-1}$ respectively, and low SSA > 30 $m^2{\cdot}g^{-1}$ and 15–20 $m^2{\cdot}g^{-1}$, respectively and average density of 3.9 $g{\cdot}cm^{-3}$ and 3.95–4.1 $g{\cdot}cm^{-3}$, respectively.

5.7 MoS_2–Al_2O_3/HOSO Hybrid Nanofluid

The thermal conductivity of MoS_2–Al_2O_3/HOSO hybrid nanofluids measurements vs temperature and nanoparticle wt% concentration is shown in Fig. 9a and b, respectively. The percentage enhancement of thermal conductivity vs wt% concentration is shown in Fig. 9c. It is observed from Fig. 9a that thermal conductivities are very low and decreases linearly with an increase in temperature for all wt%

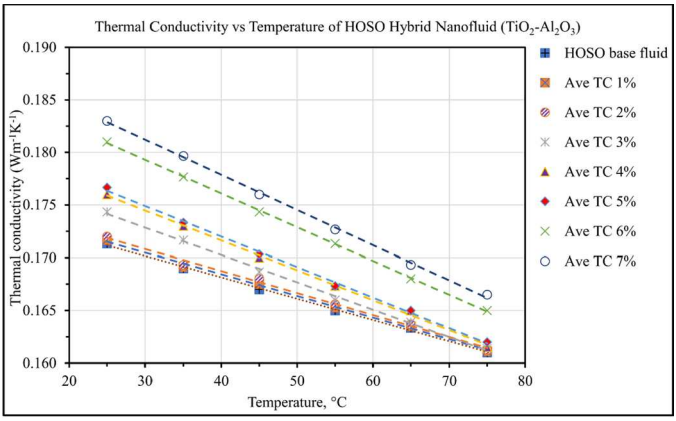

a. Thermal conductivity vs temperature.

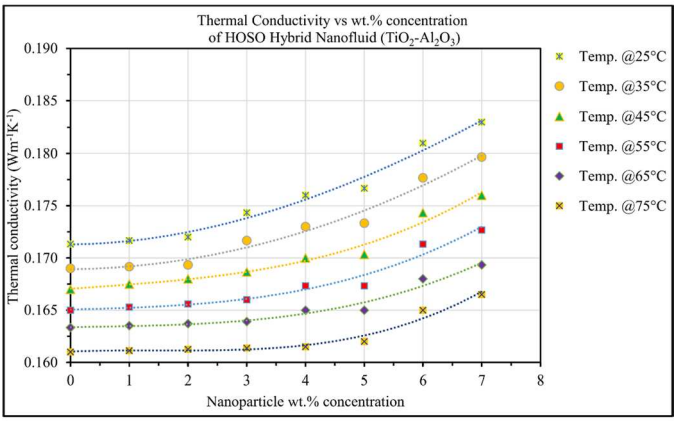

b. Thermal conductivity vs weight percentage concentration.

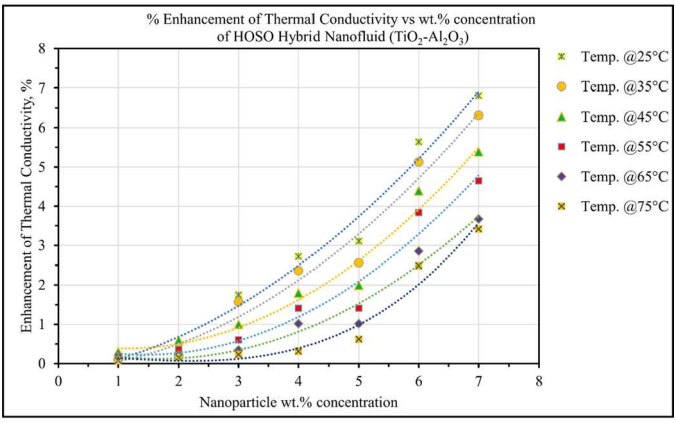

c. Enhancement of thermal conductivity vs wt.% concentration.

Fig. 8 Thermal conductivity of TiO_2–Al_2O_3/HOSO-hybrid nanofluid and base fluid

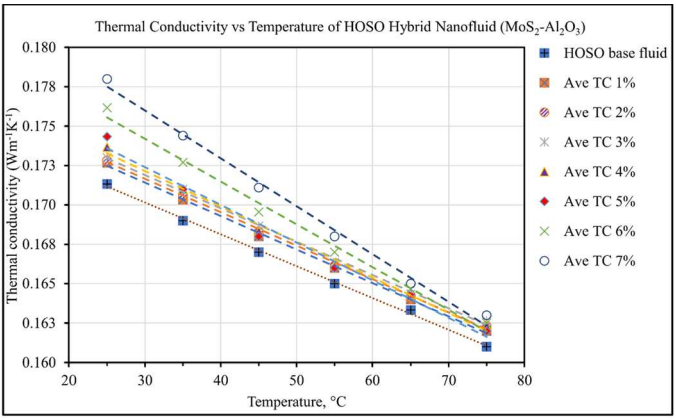

a. Thermal conductivity vs temperature.

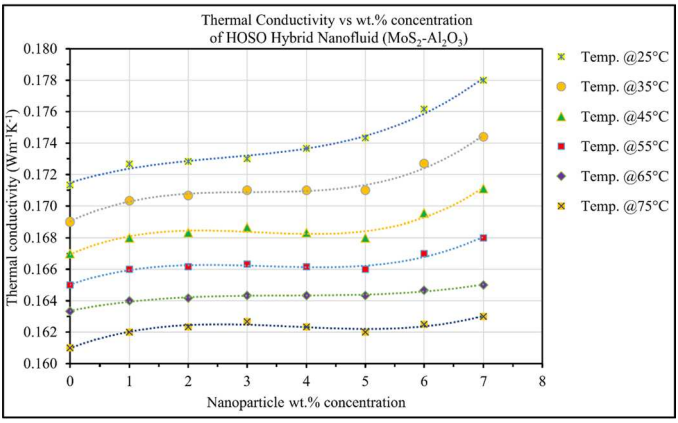

b. Thermal conductivity vs weight percentage concentration.

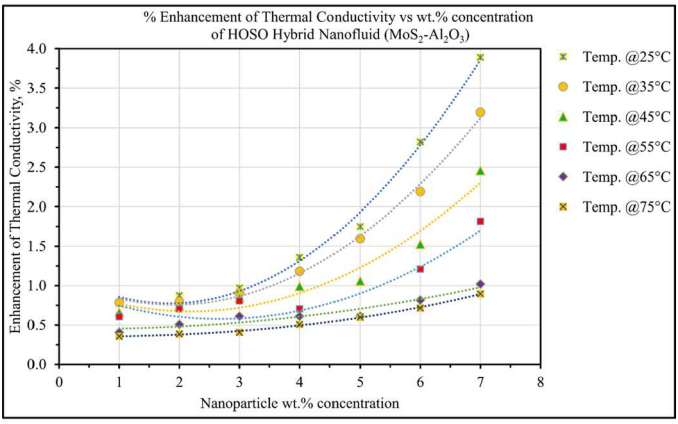

c. Enhancement of thermal conductivity vs wt.% concentration.

Fig. 9 Thermal conductivity of MoS_2–Al_2O_3/HOSO hybrid nanofluid and base fluid HOCO-based hybrid nanofluid

concentration. Figure 9b shows that the addition of MoS_2–Al_2O_3 hybrid nanoparticle to the base fluid, thermal conductivity increases very slowly and nonlinearly with increase in wt% concentration, following second order polynomial. At 1-wt% nanoparticle concentration, the thermal conductivity enhancement for MoS_2–Al_2O_3/HOSO hybrid nanofluid were 0.778 %, 0.789 %, 0.599 %, 0.606 %, 0.408 %, and 0.621 % at 25 °C, 35 °C, 45 °C, 55 °C, 65 °C, and 75 °C respectively as observed in Fig. 9c. At 7-wt% nanoparticle concentration, the thermal conductivity enhancement for MoS_2–Al_2O_3 hybrid nanofluid were 3.891 %, 2.564 %, 1.796 %, 1.212 %, 1.02 %, and 1.242 % at 25 °C, 35 °C, 45 °C, 55 °C, 65 °C, and 75 °C respectively. The thermal conductivity of MoS_2–Al_2O_3 at 25 °C for 1-wt% and 7-wt% concentrations were 0.173 $Wm^{-1}{\cdot}K^{-1}$ and 0.178 $Wm^{-1}{\cdot}K^{-1}$ respectively; and at 75 °C for 1-wt% and 7-wt% concentrations were 0.162 $Wm^{-1}{\cdot}K^{-1}$ and 0.163 $Wm^{-1}{\cdot}K^{-1}$. This low thermal conductivity and low enhancement implies there is no synergistic relationship between MoS_2 and Al_2O_3. Both nanoparticles MoS_2 and Al_2O_3 have small particle size of 30 nm, moderate thermal conductivity of 40 $Wm^{-1}{\cdot}K^{-1}$ to 50 $Wm^{-1}{\cdot}K^{-1}$ and 12 $Wm^{-1}{\cdot}K^{-1}$ to 38 $Wm^{-1}{\cdot}K^{-1}$ respectively, and low SSA 45 and 15 $m^2{\cdot}g^{-1}$ to 20 $m^2{\cdot}g^{-1}$ respectively and average density of 5.06 and 3.95 $g{\cdot}cm^{-3}$ to 4.1 $g{\cdot}cm^{-3}$ respectively.

5.8 xGnP-TiO_2/HOCO Hybrid Nanofluid

The thermal conductivity measurements of xGnP-TiO_2/HOCO hybrid nanofluid vs temperature and nanoparticle wt% concentration is shown in Fig. 10a and b, respectively. The Percentage enhancement of thermal conductivity vs wt% concentration is shown in Fig. 10c. It is observed from Fig. 10a that thermal conductivity decreases linearly with increase in temperature for all wt% concentration. Figure 10b shows that the addition of xGnP-TiO_2 hybrid nanoparticle to HOCO base fluid, thermal conductivity increases nonlinearly with increase in wt% concentration, following second order polynomial trend. There is a gradual increase between 0-wt% and 2 wt% concentration and a rapid increase between 2-wt% and 7-wt% nanoparticle concentration. At 1-wt% nanoparticle concentration, the thermal conductivity enhancement for xGnP-TiO_2/HOCO hybrid nanofluid were 13.64 %, 13.02 %, 11.18 %, 9.29 %, 7.98 %, and 7.45 % at 25 °C, 35 °C, 45 °C, 55 °C, 65 °C, and 75 °C, respectively as observed in Fig. 10c. At 7 wt% nanoparticle concentration, the thermal conductivity enhancement for xGnP-TiO_2/HOCO hybrid nanofluid were 101.36, 98.82, 98.21, 97.78, 97.14 and 97.52 at 25 °C, 35 °C, 45 °C, 55 °C, 65 °C, and 75 °C respectively. The thermal conductivity of xGnP-TiO_2/HOCO hybrid nanofluid at 25 °C for 1-wt% and 7-wt% concentrations were 0.194 $Wm^{-1}{\cdot}K^{-1}$ and 0.344 $Wm^{-1}{\cdot}K^{-1}$, respectively. This increase in thermal conductivity is a result of high thermal conductivity of xGnP-H5 nanoplatelet (3000 $Wm^{-1}{\cdot}K^{-1}$), the multilayered structure, low density of 0.03 $g{\cdot}cm^{-3}$ which makes the nanoparticle to be well dispersed and stable, small thickness of 15 nm, and large surface area ($SSA = 50$ $m^2{\cdot}g^{-1}$ to 80 $m^2{\cdot}g^{-1}$), and in combination of TiO_2 small particle size of 30 nm, low thermal conductivity of 6.8 $Wm^{-1}{\cdot}K^{-1}$ to 8.5 $Wm^{-1}{\cdot}K^{-1}$, moderate SSA > 30 $m^2{\cdot}g^{-1}$, and average density of 3.9 $g{\cdot}cm^{-3}$.

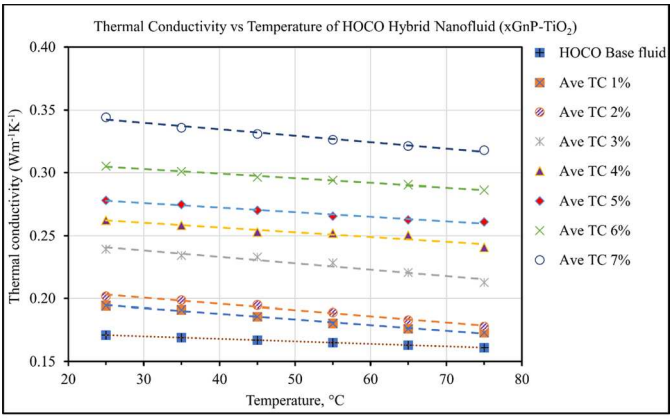

a. Thermal conductivity vs temperature.

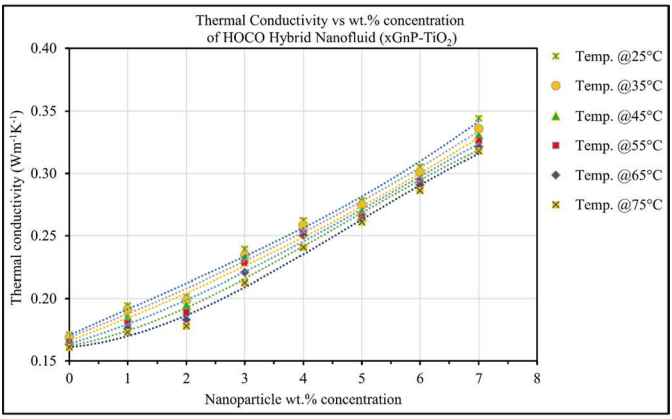

b. Thermal conductivity vs weight percentage concentration.

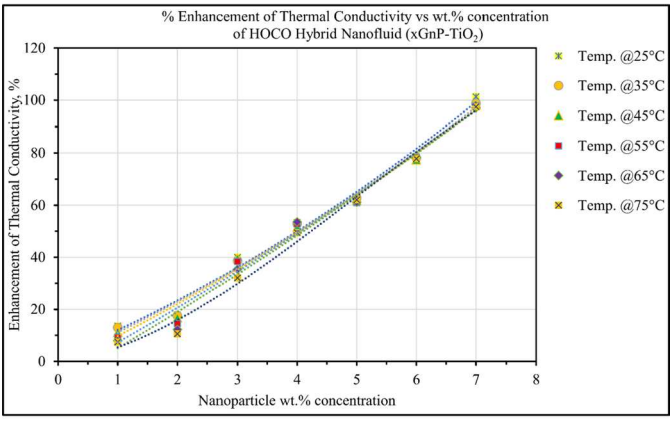

c. Enhancement of thermal conductivity vs wt.% concentration.

Fig. 10 Thermal conductivity of xGnP-TiO_2/HOCO hybrid nanofluid and base fluid

5.9 xGnP-MoS_2/HOCO Hybrid Nanofluid

The thermal conductivity of xGnP-MoS_2/HOSO hybrid nanofluids measurements vs temperature and nanoparticle wt% concentration is shown in Fig. 11a and b respectively. The Percentage enhancement of thermal conductivity vs wt% concentration is shown in Fig. 11c. It is observed from Fig. 11a that thermal conductivity decreases linearly with an increase in temperature for all wt% concentrations. Figure 11b shows that the addition of xGnP-MoS_2 hybrid nanoparticle to the base fluid, thermal conductivity increases nonlinearly with increase in wt% concentration, following second order polynomial trend. At 1-wt% nanoparticle concentration, the thermal conductivity enhancement for xGnP-MoS_2/HOCO hybrid nanofluid were 16.18 %, 15.36 %, 13.97 %, 11.52 %, 10.63 %, and 9.11 % at 25 °C, 35 °C, 45 °C, 55 °C, 65 °C, and 75 °C respectively as observed in Fig. 11c. At 7-wt% nanoparticle concentration, the thermal conductivity enhancement for xGnP-MoS_2/HOCO hybrid nanofluid were 101.36 %, 98.82 %, 98.20 %, 97.77 %, 97.14 %, and 97.52% at 25 °C, 35 °C, 45 °C, 55 °C, 65 °C, and 75 °C, respectively. It is also observed that at higher wt% concentration from 5-wt% to 7-wt% concentration there is rapid enhancement, and the effect of temperature is minimized. The thermal conductivity of xGnP-MoS_2/HOCO hybrid nanofluid at 25 °C for 1-wt% and 7-wt% concentrations were 0.199 $Wm^{-1}\cdot K^{-1}$ and 0.34 $Wm^{-1}\cdot K^{-1}$ respectively. This increase in thermal conductivity is explained under xGnP-MoS_2/HOSO.

5.10 xGnP-Al_2O_3/HOCO Hybrid Nanofluid

The thermal conductivity of xGnP-Al_2O_3/HOCO hybrid nanofluids measurements vs temperature and nanoparticle wt% concentration is shown in Fig. 12a and b, respectively. The percentage enhancement of thermal conductivity vs wt% concentration is shown in Fig. 12c. It is observed from Fig. 12a that thermal conductivity decreases linearly with an increase in temperature for all wt% concentrations. Figure 12b shows that the addition of xGnP-Al_2O_3 hybrid nanoparticle to the base fluid, thermal conductivity increases nonlinearly with increase in wt% concentration, following second order polynomial trend. At 1-wt% nanoparticle concentration, the thermal conductivity enhancement for xGnP-Al_2O_3/HOCO hybrid nanofluid were 15.2 %, 14.0 %, 11.38 %, 9.29 %, 7.98 %, and 7.45 % at 25 °C, 35 °C, 45 °C, 55 °C, 65 °C, and 75 °C respectively as observed in Fig. 12c. At 7-wt% nanoparticle concentration, the thermal conductivity enhancement for xGnP-Al_2O_3/HOCO hybrid nanofluid were 91.62, 89.94, 88.02, 86.26, 84.46, and 83.23% at 25, 35, 45, 55, 65, and 75 °C, respectively. It is also observed that at 3, 4, and 6 wt% concentration the effect of temperature is minimized. The thermal conductivity of xGnP-Al_2O_3/HOCO at 25 °C for 1 and 7-wt% concentrations were 0.197 $Wm^{-1}\cdot K^{-1}$ and 0.33 $Wm^{-1}\cdot K^{-1}$ respectively; and at 75 °C for 1 and 7-wt% concentrations were 0.161 $Wm^{-1}\cdot K^{-1}$ and 0.29 $Wm^{-1}\cdot K^{-1}$, respectively. This increase in thermal conductivity is explained under xGnP-Al_2O_3/HOCO.

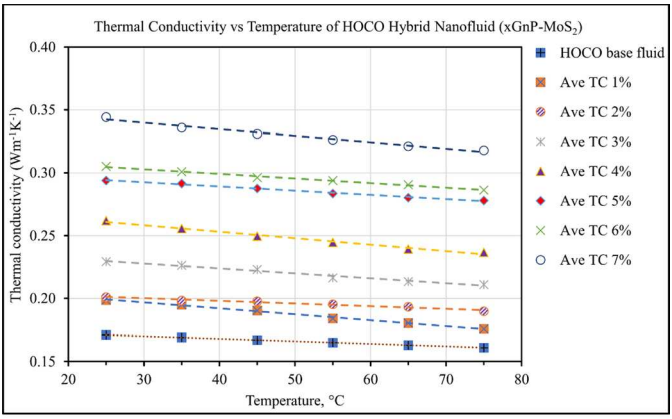

a. Thermal conductivity vs temperature.

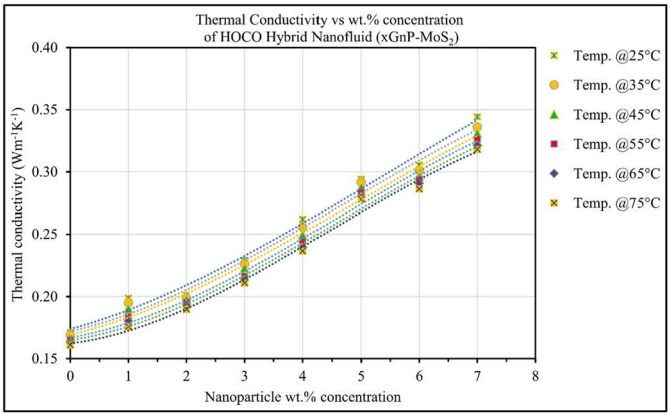

b. Thermal conductivity vs weight percentage concentration.

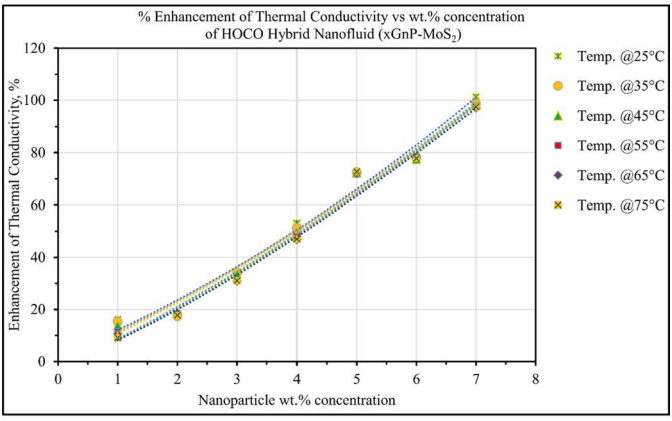

c. Enhancement of thermal conductivity vs wt.% concentration.

Fig. 11 Thermal conductivity of xGnP-MoS_2/HOCO hybrid nanofluid and base fluid

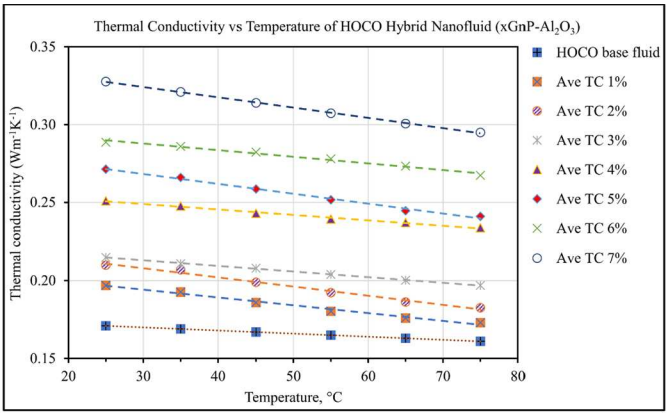

a. Thermal conductivity vs temperature.

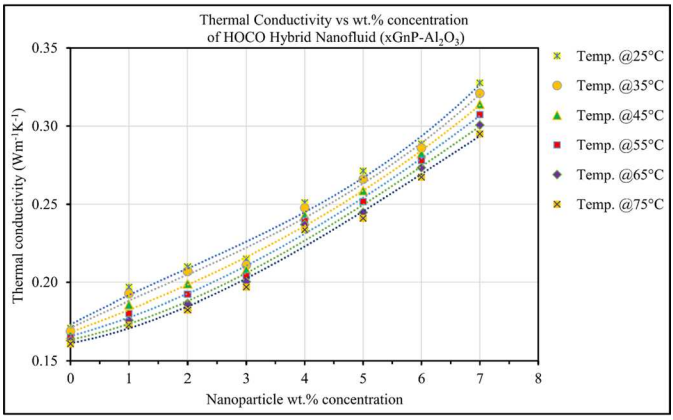

b. Thermal conductivity vs weight percentage concentration.

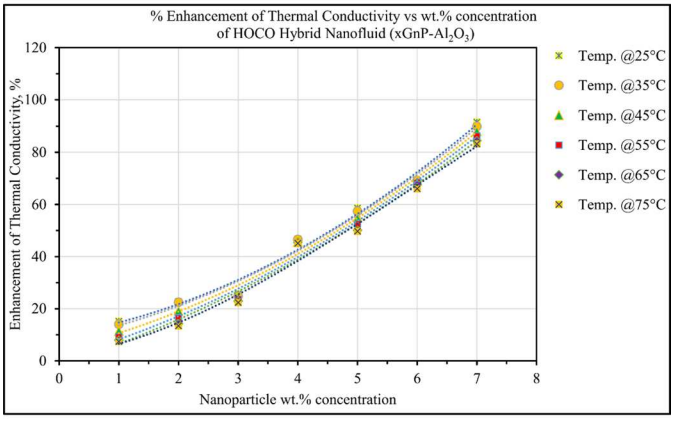

c. Enhancement of thermal conductivity vs wt.% concentration.

Fig. 12 Thermal conductivity of xGnP-Al_2O_3/HOCO hybrid nanofluid and base fluid

5.11 TiO_2–MoS_2/HOSO Hybrid Nanofluid

The thermal conductivity of TiO_2–MoS_2/HOCO hybrid nanofluids measurements vs temperature and nanoparticle wt% concentration is shown in Fig. 13a and b respectively. The Percentage enhancement of thermal conductivity vs wt% concentration is shown in Fig. 13c. It is observed from Fig. 13a that thermal conductivities are very low and decrease linearly with an increase in temperature for all wt% concentration. Figure 13b shows that the addition of TiO_2–MoS_2 hybrid nanoparticle to the base fluid, thermal conductivity increases very slowly and nonlinearly with an increase in wt% concentration, following second order polynomial trend. At 1-wt% nanoparticle concentration, the thermal conductivity enhancement for TiO_2–MoS_2/HOCO hybrid nanofluid were 1.17 %, 1.18 %, 0.599 %, 0.4 %, 1.24E−06 %, and 0.0 % at 25 °C, 35 °C, 45 °C, 55 °C, 65 °C, and 75 °C respectively as observed in Fig. 13c. At 7-wt% nanoparticle concentration, the thermal conductivity enhancement for TiO_2–MoS_2/HOCO hybrid nanofluid were 6.04 %, 5.52 %, 4.79 %, 4.24 %, 3.89 %, and 3.83 % at 25 °C, 35 °C, 45 °C, 55 °C, 65 °C, and 75 °C respectively. It is also observed that temperature has significant effect at all wt% concentration. The thermal conductivity of TiO_2–MoS_2/HOCO at 25 °C for 1-wt% and 7-wt% concentrations were 0.173 $Wm^{-1}{\cdot}K^{-1}$ and 0.181 $Wm^{-1}{\cdot}K^{-1}$ respectively; and at 75 °C for 1-wt% and 7-wt% concentrations were 0.161 $Wm^{-1}{\cdot}K^{-1}$ and 0.167 $Wm^{-1}{\cdot}K^{-1}$. This low thermal conductivity and low enhancement implies there is no synergistic relationship between TiO_2 and MoS_2 as explained under TiO_2–MoS_2/HOSO.

Since TiO_2–MoS_2/HOSO, TiO_2–Al_2O_3/HOSO, MoS_2–Al_2O_3/HOSO and TiO_2–MoS_2/HOCO based nanofluids showed similar and insignificant enhancements in thermal conductivity of the base fluid, TiO_2–Al_2O_3/HOCO and MoS_2–Al_2O_3/HOCO experiment were discontinued.

5.11.1 xGnP/HOSO Mono Nanofluid

The % enhancement of TC of xGnP/HOSO mono nanofluid increased significantly and nonlinearly with increase of wt% concentration as shown in Fig. 14. Thermal conductivity of xGnP/HOSO mono nanofluid at 25 °C and 75 °C at 7-wt% concentration of xGnP nanoplatelet is 0.53 $Wm^{-1}{\cdot}K^{-1}$ and 0.47 $Wm^{-1}{\cdot}K^{-1}$, respectively, while at 1-wt% are 0.21 $Wm^{-1}{\cdot}K^{-1}$ and 0.19 $Wm^{-1}{\cdot}K^{-1}$, respectively.

At 25 °C thermal conductivity enhancement for wt% concentrations at 1, 2, 3, 4, 5, 6, and 7 are 25 %, 54 %, 75 %, 106 %, 171 %, 191 %, and 214 %, respectively, while at 75 °C, the enhancement are 22 %, 52 %, 74 %, 104 %, 172 %, 177 %, and 196 %. It was observed that there is no synergistic relationship between graphene nanoplatelet and TiO_2, MoS_2 and Al_2O_3, instead graphene is improving the performance of TiO_2, MoS_2 and Al_2O_3 in the base fluid. Therefore, thermal conductivity of the hybrid nanofluids is lower to more than one order compared to mono nanofluids.

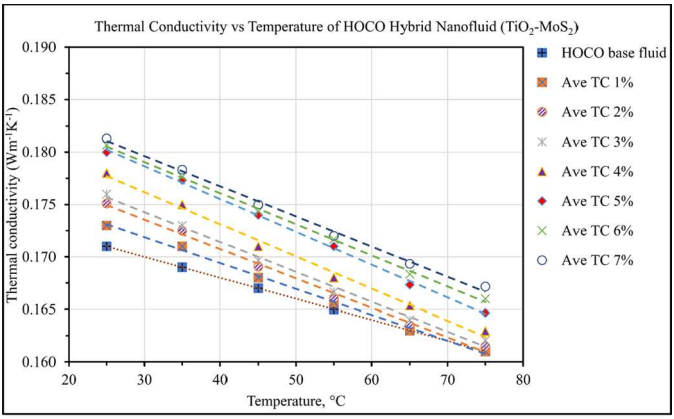

a. Thermal conductivity vs temperature.

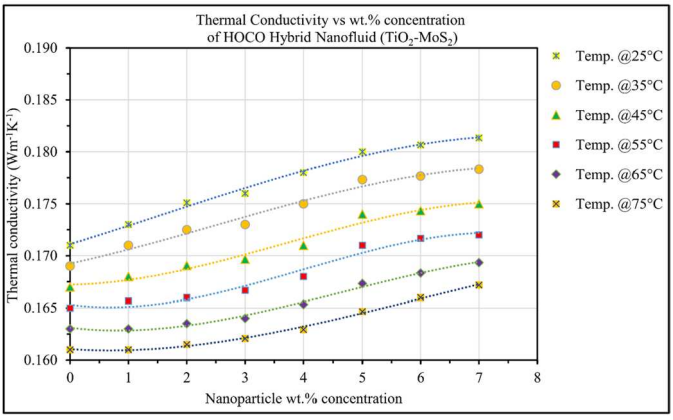

b. Thermal conductivity vs weight percentage concentration.

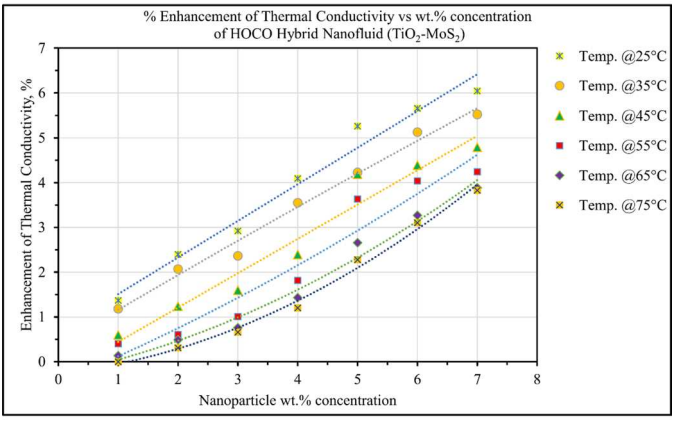

c. Enhancement of thermal conductivity vs wt.% concentration.

Fig. 13 Thermal conductivity of TiO_2–MoS_2/HOCO hybrid nanofluid and base fluid

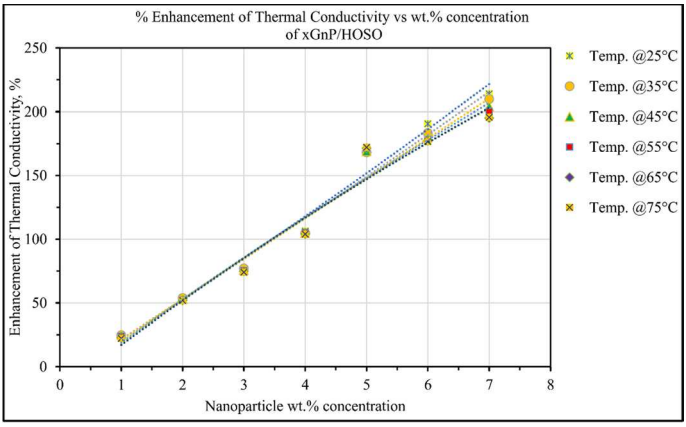

Fig. 14 % Enhancement of TC vs wt% concentration of xGnP/HOSO nanofluid

5.12 Comparative Plots of Thermal Conductivity of all Hybrid Nanofluids

Comparative plots for HOSO and HOCO based hybrid nanofluids are shown in Figs. 15 and 16. At 7-wt% concentration and 25 °C, xGnP-TiO_2/HOSO gave the highest thermal conductivity enhancement (109.73 %) followed by xGnP-TiO_2/HOCO (101.36 %), xGnP-MoS_2/HOCO (101.36 %), xGnP-MoS_2/HOSO (96.30 %), xGnP-Al_2O_3/HOCO (91.62 %), xGnP-Al_2O_3/HOSO (91.25 %), TiO_2–MoS_2/HOSO (7 %), TiO_2–Al_2O_3/HOSO (6.81 %), TiO_2–MoS_2/HOCO (6.04 %), MoS_2–Al_2O_3/HOSO (3.89 %).

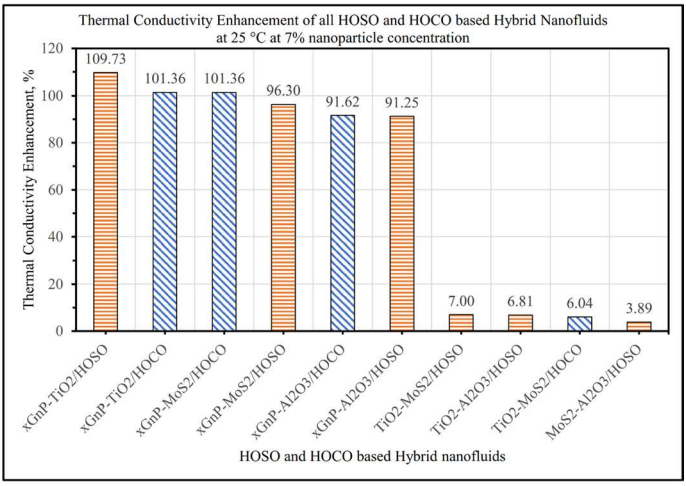

Fig. 15 HOSO and HOCO based nanofluids at 7 wt% concentration at 25 °C

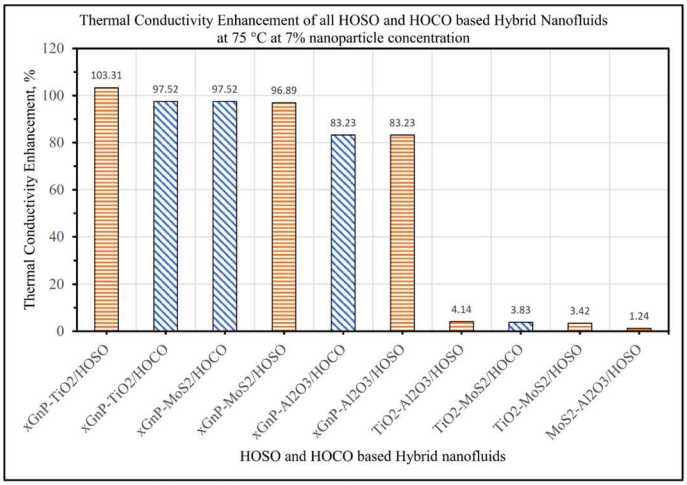

Fig. 16 HOSO and HOCO-based nanofluids at 7-wt% concentration at 75 °C

At 7-wt% concentration and 75 °C, xGnP-TiO_2/HOSO gave the highest thermal conductivity enhancement (103.31%) followed by xGnP-TiO_2/HOCO (97.52%), xGnP-MoS_2/HOCO (97.52%), xGnP-MoS_2/HOSO (96.89%), xGnP-Al_2O_3/HOCO (83.23%), xGnP-Al_2O_3/HOSO (83.23%), TiO_2–Al_2O_3/HOSO (4.14%), TiO_2-MoS_2/HOCO (3.83%), TiO_2-MoS_2/HOSO (3.42%), MoS_2–Al_2O_3/HOSO (1.24%).

6 Conclusions

Six HOSO- and four HOCO-based hybrid nanofluids were formulated with four different types of nanoparticles (Graphene nanoplatelet (XGnP), TiO_2, MoS_2, and Al_2O_3) at varying nanoparticles wt% concentration from 1 % to 7 % in 1 % increment using the two-step method to obtain xGnP-TiO_2/HOSO, xGnP-MoS_2/HOSO, xGnP-Al_2O_3/HOSO, TiO_2–MoS_2/HOSO, TiO_2–Al_2O_3/HOSO MoS_2–Al_2O_3/HOSO, xGnP-TiO_2/HOCO, xGnP-MoS_2/HOCO, xGnP-Al_2O_3/HOCO, and TiO_2–MoS_2/HOCO hybrid nanofluids as well as xGnP-TiO_2/HOSO mono nanofluid for comparison. Thermal conductivity of the formulated nanofluids were measured and characterized vs temperature and nanoparticle wt% concentration for use in MQL machining of difficult-to-cut metals. From the results, the following conclusions can be made:

1. Thermal conductivity of all nanofluids decreases linearly with temperature, while the thermal conductivity enhancement increases nonlinearly with an increase in wt% concentration, following second order polynomial trend.
2. Amid all nanofluids, at 7-wt% concentration of nanoparticles, xGnP-TiO_2/HOSO gave the highest thermal conductivity enhancement (109.73 and 103.31 at 25 °C and 75 °C), followed by xGnP-TiO_2/HOCO (101.36 and 97.52 at 25 °C

and 75 °C), xGnP-MoS_2/HOCO (101.36 % and 97.52 % at 25 °C and 75 °C), xGnP-MoS_2/HOSO (96.3 % and 96.89 % at 25 °C and 75 °C), xGnP-Al_2O_3/HOCO (91.62 and 83.23% at 25 °C and 75 °C), xGnP-Al_2O_3/HOSO (91.25 % and 83.23 % at 25 °C and 75 °C).

3. The high thermal conductivity of xGnP-dispersed nanofluids is due to the high thermal conductivity of graphene nanoplatelet (3000 W), high surface area of the nanoplatelet, and higher Brownian motion of the suspended nanoparticles which is inversely proportional to the density of the particles.
4. xGnP-TiO_2/HOSO, xGnP-TiO_2/HOCO, xGnP-MoS_2/HOCO, and xGnP-MoS_2/HOSO are strongly recommended in MQL machining. Also, xGnP-Al_2O_3/HOCO and xGnP-Al_2O_3/HOSO are recommended due to improved tribological properties of Al_2O_3.
5. TiO_2–MoS_2/HOSO, TiO_2–Al_2O_3/HOSO hybrid nanofluids gave the lowest thermal conductivities enhancement of (0.78 % at 1 wt% and 7 % at 7 wt% concentration at 25 °C), and (0.194 % at 1 wt% and 6.81 % at 7 wt% concentration at 25 °C), respectively.
6. TiO_2–MoS_2/HOSO, TiO_2–Al_2O_3/HOSO hybrid nanofluids are not recommended as base fluids due to their insignificant enhancement of thermal conductivity of vegetable oil base fluids.
7. There is no synergy in mixing metallic–non-metallic–oxides or metallic oxide and MoS_2 in the base fluid for MQL machining, for they show insignificant improvement in thermal conductivity of the base fluid.
8. Thermal conductivity of the hybrid nanofluids is lower to more than one order compared to mono nanofluids.

7 Recommendation for Further Work

Further work is recommended to investigate the performance of the identified good performing hybrid nanofluids in actual machining of difficult-to-cut metals such as Inconel-718, Compacted Graphite Iron (CGI). The effect of cooling strategies on cutting forces, surface roughness, tool wear, and residual stresses will be investigated using xGnP-TiO_2/HOSO, xGnP-TiO_2/HOCO, xGnP-MoS_2/HOCO, xGnP-MoS_2/HOSO, xGnP-Al_2O_3/HOCO and xGnP-Al_2O_3/HOSO nanofluids at 7 wt% concentration.

Acknowledgments The authors acknowledge the financial support of the National Science Foundation under Grant number NSF CMMI2218786. The financial support from the Intelligent System Center (ISC) and the Department of Mechanical and Aerospace Engineering, Missouri University of Science and Technology are also greatly acknowledged. The supply of high oleic soybean oil samples from Archer Daniels Midland Inc., and Cargill Inc, USA and Low Oleic soybean oil samples from Welch Holme and Clark (Newark, NJ, USA) are greatly acknowledged. Some of the experimental data were collected by Ali Nasrabadi is also acknowledged.

Author Contributions All authors contributed to the study, conception and design. Material preparation, data collection and analysis were performed by Anthony C Okafor and Tobechukwu K. Abor. The first draft of the manuscript was written by Anthony C. Okafor and Saidanvar E. Valiev. Ignatius Ekengwu,

Abiodun Saka and Monday U. Okoronkwo commented on previous versions of the manuscript. All authors read and approved the final manuscript.

Funding The authors acknowledge the financial support of the National Science Foundation under Grant number NSF CMMI2218786. The financial support from the Intelligent System Center (ISC) and the Department of Mechanical and Aerospace Engineering, Missouri University of Science and Technology are also greatly acknowledged. The supply of high oleic soybean oil and high oleic canola oil samples from Archer Daniels Midland Inc., and Cargill Inc, USA are greatly acknowledged.

Data Availability No datasets were generated or analysed during the current study.

Declarations

Competing Interests The authors declare that they have no known competing financial interests or personal relationships that could have appeared to influence the work reported in this paper.

References

1. B.N. Bhat, *Aerospace materials and applications* (American Institute of Aeronautics and Astronautics, Reston, 2018), pp.11–208
2. A.S. Patil, S.V. Ingle, Y.S. More, M.S. Mathe, Int. J. Innov. Eng. Technol. (IJIET) **5**, 139–144 (2015)
3. B.L. Tai, J.M. Dasch, A.J. Shih, Mach. Sci. Technol. **15**, 376–391 (2011). https://doi.org/10.1080/10910344.2011.620910
4. M. Becker, *Viscosity of Metalworking Fluids in Cutting Processes Determined with SVM™ 3001 or SVM™ 4001 Viscometer* (Anton Paar, 2018), https://www.muser-my.com/wp-content/uploads/2018/11/D89IA020EN-B_AppRep_CuttingFluids.pdf. Accessed 27 July 2024
5. K. Zheng Yang, A. Pramanik, A.K. Basak, Y. Dong, C. Prakash, S. Shankar, S. Dixit, K. Kumar, N. Ivanovich Vatin, Ain Shams Eng. J. **14**, 101–119 (2023)
6. A.C. Okafor, T.O. Nwoguh, Int. J. Adv. Manuf. Technol. **106**, 2137–2145 (2020). https://doi.org/10.1007/s00170-019-04611-3
7. S. Valiev, A.C. Okafor, A. Prakash Hungund, J. Huang, Eng. Fail. Anal. **157**, 107887 (2024). https://doi.org/10.1016/j.engfailanal.2023.107887
8. M.S. Najiha, M.M. Rahman, A.R. Yusoff, Renew. Sustain. Energy Rev. **60**, 1008–1031 (2016)
9. J.M.D. Bruce, L. Tai, A.J. Shih, Mach. Sci. Technol. **15**, 376–391 (2011). https://doi.org/10.1080/10910344.2011.620910
10. A. Shokrani, V. Dhokia, S.T. Newman, J. Manuf. Process. **21**, 99–108 (2016). https://doi.org/10.1016/j.jmapro.2015.12.002
11. A.C. Okafor, P.M. Jasra, Int. J. Mach. Machin. Mater. **21**, 1–15 (2019). https://doi.org/10.1504/ijmmm.2019.098065
12. K.H. Park, M.A. Suhaimi, G.D. Yang, D.Y. Lee, S.W. Lee, P. Kwon, Int. J. Precis. Eng. Manuf. **18**, 5–10 (2017). https://doi.org/10.1007/s12541-017-0001-z
13. M.A. Haq, S. Hussain, M.A. Ali, M.U. Farooq, N.A. Mufti, C.I. Pruncu, A. Wasim, J. Clean. Prod. **310**, 127463 (2021). https://doi.org/10.1016/j.jclepro.2021.127463
14. G. Li, S. Yi, N. Li, W. Pan, C. Wen, S. Ding, J. Mater. Process. Technol. **271**, 62–72 (2019). https://doi.org/10.1016/j.jmatprotec.2019.04.035
15. M. Chandrasekar, S. Suresh, A. Chandra Bose, Exp. Therm. Fluid Sci. **34**, 210–216 (2010). https://doi.org/10.1016/j.expthermflusci.2009.10.022
16. A. Turgut, I. Tavman, M. Chirtoc, H.P. Schuchmann, C. Sauter, S. Tavman, Int. J. Thermophys. **30**, 1213–1226 (2009). https://doi.org/10.1007/s10765-009-0594-2
17. R.S. Vajjha, D.K. Das, Int. J. Heat Mass Transf. **52**, 4675–4682 (2009). https://doi.org/10.1016/j.ijheatmasstransfer.2009.06.027
18. A. Sharma, R.C. Singh, R.M. Singari, and S.L. Bhandarkar, in *Lect Notes Mech Eng*, pp. 1–12 (2022).

19. S. Yuan, X. Hou, L. Wang, B. Chen, Tribol. Lett. **66**, 117 (2018). https://doi.org/10.1007/s11249-018-1059-1
20. Y. Zhang, C. Li, D. Jia, D. Zhang, X. Zhang, J. Clean. Prod. **87**, 930–940 (2015). https://doi.org/10.1016/j.jclepro.2014.10.027
21. T.M. Duc, T.T. Long, N.M. Tuan, Lubricants **9**, 45 (2021). https://doi.org/10.3390/lubricants9040045
22. T.M. Duc, T.T. Long, N.M. Tuan, Fluids **6**, 248 (2021). https://doi.org/10.3390/fluids6070248
23. B. Sen, M. Mia, M.K. Gupta, M.A. Rahman, U.K. Mandal, S.P. Mondal, Int. J. Adv. Manuf. Technol. **103**, 119–130 (2019). https://doi.org/10.1007/s00170-019-03814-y
24. F.E. Berger Bioucas, M.H. Rausch, J. Schmidt, A. Bück, T.M. Koller, A.P. Fröba, Int. J. Thermophys. **41**, 62 (2020). https://doi.org/10.1007/s10765-020-2621-2
25. M. Asadi, A. Asadi, S. Aberoumand, Int. J. Refrig. **89**, 83–90 (2018). https://doi.org/10.1016/j.ijrefrig.2018.03.014
26. A.N. Omrani, E. Esmaeilzadeh, M. Jafari, A. Behzadmehr, Diam. Relat. Mater. **93**, 1–7 (2019). https://doi.org/10.1016/j.diamond.2019.02.002
27. S. Sreekumar, A. Ganguly, S. Khalil, S. Chakrabarti, N. Hewitt, J.D. Mondol, N. Shah, J. Clean. Prod. **434**, 140395 (2024). https://doi.org/10.1016/j.jclepro.2023.140395
28. A. Kumar Sharma, A. Kumar Tiwari, A. Rai Dixit, R. Kumar Singh, Measurement (Lond) **150**, 107078 (2020). https://doi.org/10.1016/j.measurement.2019.107078
29. M. Jamil, A.M. Khan, H. Hegab, M.K. Gupta, M. Mia, N. He, G. Zhao, Q. Song, Z. Liu, Int. J. Adv. Manuf. Technol. **107**, 2317–2330 (2020). https://doi.org/10.1007/s00170-020-05296-9
30. P.S. Azharuddin, Int. J. Thermophys. **45**, 83 (2024). https://doi.org/10.1007/s10765-024-03377-5
31. M. Hemmat Esfe, M. Bahiraei, A. Mir, Adv. Colloid Interface Sci. **282**, 102208 (2020)
32. Ş Şirin, T. Kıvak, J. Manuf. Process. **70**, 78–90 (2021). https://doi.org/10.1016/j.jmapro.2021.08.038
33. A. Asadi, M. Asadi, M. Siahmargoi, T. Asadi, M. Gholami Andarati, Int. J. Heat Mass Transf. **108**, 1910–1915 (2017). https://doi.org/10.1016/j.ijheatmasstransfer.2016.12.022
34. T.O. Nwoguh, A.C. Okafor, H.A. Onyishi, Int. J. Adv. Manuf. Technol. **113**, 2137–2145 (2021). https://doi.org/10.1007/s00170-021-06812-1

Authors and Affiliations

Anthony Chukwujekwu Okafor[1] · Tobechukwu Kingsley Abor[1] · Saidanvar Esanjonovich Valiev[1] · Ignatius Echezona Ekengwu[1] · Abiodun Saka[2] · Monday U. Okoronkwo[2]

✉ Anthony Chukwujekwu Okafor
okafor@mst.edu

[1] Computer Numeric Control and Virtual Manufacturing Laboratory, Department of Mechanical and Aerospace Engineering, Missouri University of Science and Technology, 327 Toomey Hall, Rolla, MO 65409-005, USA

[2] Sustainable Materials Laboratory, Linda and Bipin Doshi Department of Chemical and Biochemical Engineering, Missouri University of Science and Technology, Rolla, MO 65409, USA